

Wilfrid Laurier University

Scholars Commons @ Laurier

Theses and Dissertations (Comprehensive)

2010

Mathematical Modeling and Control of Nonlinear Oscillators with Shape Memory Alloys

Mohamed Bendame
Wilfrid Laurier University

Follow this and additional works at: <https://scholars.wlu.ca/etd>



Part of the [Mathematics Commons](#)

Recommended Citation

Bendame, Mohamed, "Mathematical Modeling and Control of Nonlinear Oscillators with Shape Memory Alloys" (2010). *Theses and Dissertations (Comprehensive)*. 992.
<https://scholars.wlu.ca/etd/992>

This Thesis is brought to you for free and open access by Scholars Commons @ Laurier. It has been accepted for inclusion in Theses and Dissertations (Comprehensive) by an authorized administrator of Scholars Commons @ Laurier. For more information, please contact scholarscommons@wlu.ca.



Library and Archives
Canada

Published Heritage
Branch

395 Wellington Street
Ottawa ON K1A 0N4
Canada

Bibliothèque et
Archives Canada

Direction du
Patrimoine de l'édition

395, rue Wellington
Ottawa ON K1A 0N4
Canada

Your file *Votre référence*
ISBN: 978-0-494-68720-8
Our file *Notre référence*
ISBN: 978-0-494-68720-8

NOTICE:

The author has granted a non-exclusive license allowing Library and Archives Canada to reproduce, publish, archive, preserve, conserve, communicate to the public by telecommunication or on the Internet, loan, distribute and sell theses worldwide, for commercial or non-commercial purposes, in microform, paper, electronic and/or any other formats.

The author retains copyright ownership and moral rights in this thesis. Neither the thesis nor substantial extracts from it may be printed or otherwise reproduced without the author's permission.

In compliance with the Canadian Privacy Act some supporting forms may have been removed from this thesis.

While these forms may be included in the document page count, their removal does not represent any loss of content from the thesis.

AVIS:

L'auteur a accordé une licence non exclusive permettant à la Bibliothèque et Archives Canada de reproduire, publier, archiver, sauvegarder, conserver, transmettre au public par télécommunication ou par l'Internet, prêter, distribuer et vendre des thèses partout dans le monde, à des fins commerciales ou autres, sur support microforme, papier, électronique et/ou autres formats.

L'auteur conserve la propriété du droit d'auteur et des droits moraux qui protège cette thèse. Ni la thèse ni des extraits substantiels de celle-ci ne doivent être imprimés ou autrement reproduits sans son autorisation.

Conformément à la loi canadienne sur la protection de la vie privée, quelques formulaires secondaires ont été enlevés de cette thèse.

Bien que ces formulaires aient inclus dans la pagination, il n'y aura aucun contenu manquant.


Canada

Mathematical Modeling and Control of Nonlinear Oscillators with Shape Memory Alloys

by

© Mohamed Bendame

A thesis submitted to the
Department of Mathematics
in partial fulfilment of the
requirements for the degree of
Master of Science in Applied Mathematics

Wilfrid Laurier University

September 2010

© Mohamed Bendame

Abstract

Shape memory alloys (SMAs) belong to an interesting type of materials that have attracted the attention of scientists and engineers over the last few decades. They have some interesting properties that made them the subject of extensive research to find the best ways to utilize them in different engineering, biomedical, and scientific applications. In this thesis, we develop a mathematical model and analyze the behavior of SMAs by considering a one degree of freedom nonlinear oscillator consisting of a mass connected to a fixed frame through a viscous damping and a shape memory alloy device. Due to the nonlinear and dissipative nature of shape memory alloys, optimal control and Lyapunov stability theories are used to design a controller to stabilize the response of the one degree of freedom nonlinear oscillator. Since SMAs exist in two phases, martensite and austenite, and their phase transformations are dependent on stress and temperature, this work is presented in two parts. The first part deals with the nonlinear oscillator system in its two separate phases by considering a temperature where the SMA exists in only one of the phases. A model for each phase is developed based on Landau-Ginzburg-Devonshire theory that defines the free energy in a polynomial form enabling us to describe the SMAs shape memory effect and pseudoelasticity. However, due to the phenomenon of hysteresis in SMAs, the response of the nonlinear oscillator with a SMA element, in either phase, is chaotic and unstable. In order to stabilize the chaotic behavior, an optimal linear quadratic regulator controller is designed around a stable equilibrium for the martensitic and the austenitic phases. The closed-loop response for each phase is then simulated and computational results are presented. The second part of the thesis deals with the entire system in its dynamics by combining the two phases and

taking into account the effect of temperature on the response of the system. Governing equations for the system's thermo-mechanical dynamics are constructed using conservation laws of mass, momentum, and energy. Due to the complexity of the derived thermo-mechanical model, and the need to control the nonlinear oscillator, a model reduction based on the Galerkin method is applied to the new system in order to derive a low-dimensional model which is then solved numerically. A linear feedback control strategy for nonlinear systems is then implemented to design a tracking controller that makes the system follow a given reference input signal. The work presented in this thesis demonstrates how SMAs can be modeled by using efficient methodologies in order to capture their behavior, and how SMAs can be made stable and their chaotic behavior can be controlled by using linear and nonlinear control methods.

Acknowledgements

In the name of GOD the most Gracious most Merciful.

I would like to express my sincere gratitude to Professor Roderick Melnik, my supervisor, for his guidance and tremendous support during my research. Without his help and support, it would have been impossible to accomplish this work. I am also grateful to my wife Amal and our children Younus, Yasmine and babe Adam for their patience with me throughout the years, and their support when I needed it most. I would also like to thank my mother from the bottom of my heart, and I pray to GOD to protect her always. She has been a beacon of light that lights my way, and I pray that her light will continue to shine as long as I live. She will always be in my heart.

Contents

| | | |
|----------|---|-----------|
| 1 | Introduction | 1 |
| 1.1 | Shape Memory Alloys | 2 |
| 1.2 | Overview of Constitutive Models for SMAs | 3 |
| 1.2.1 | The Polynomial Model | 3 |
| 1.2.2 | The Exponential Model | 4 |
| 1.2.3 | The Trigonometric Model | 5 |
| 1.2.4 | The Model Based on the Fermi-Dirac Statistics | 6 |
| 1.2.5 | The Fremond Model | 8 |
| 1.3 | Numerical Implementations | 9 |
| 1.4 | Historical Notes | 10 |
| 1.5 | Thesis Outline | 12 |
| 1.6 | Summary | 13 |
| 2 | Dissipative Systems and General Properties of Shape Memory Al- | |
| | loys | 15 |
| 2.1 | Dissipative Systems | 16 |
| 2.2 | Dissipative Systems in an Input/State/Output Setting | 18 |

| | | |
|----------|--|-----------|
| 2.3 | General Properties of SMAs | 21 |
| 2.3.1 | Shape memory effect | 23 |
| 2.3.2 | Superelasticity of SMAs | 25 |
| 2.4 | Summary | 26 |
| 3 | Mathematical Modeling of Nonlinear Oscillators with Shape Mem- ory Alloys at Constant Temperature | 28 |
| 3.1 | Mathematical Model of a Nonlinear Oscillator with a SMA | 29 |
| 3.2 | Analysis of the Martensitic Phase | 30 |
| 3.3 | Analysis of the Austenitic Phase | 33 |
| 3.4 | Summary | 36 |
| 4 | Optimal Control | 37 |
| 4.1 | Linear Quadratic Regulator Control Design | 40 |
| 4.2 | System Linearization | 42 |
| 4.2.1 | State-Variable Form | 43 |
| 4.2.2 | Finding Equilibria | 44 |
| 4.2.3 | Stability Check | 44 |
| 4.3 | Controllability and Observability | 45 |
| 4.4 | LQR Design of the Martensite Phase | 46 |
| 4.5 | Closed-loop Feedback Response of the Martensitic Phase | 49 |
| 4.6 | Stability by Lyapunov Method | 51 |
| 4.7 | LQR Design of the Austenitic Phase | 52 |
| 4.8 | Closed-loop Feedback Response of the Austenitic Phase | 53 |
| 4.9 | Summary | 55 |

| | | |
|----------|---|-----------|
| 5 | Thermo-mechanical Modeling of SMAs and Model Reductions | 57 |
| 5.1 | Mathematical Model of SMAs | 58 |
| 5.1.1 | Stress–Strain Relation | 59 |
| 5.1.2 | Heat Conduction | 59 |
| 5.2 | Model Simplification via Galerkin Model Reduction | 61 |
| 5.2.1 | Galerkin Projection | 62 |
| 5.2.2 | Galerkin Method | 63 |
| 5.2.3 | Reduced Order Model | 65 |
| 5.3 | Computational Results | 66 |
| 5.4 | Thermo-mechanical SMA Model Based on Fermi-Dirac Theory | 70 |
| 5.4.1 | Phase Transformations | 71 |
| 5.4.2 | Temperature Dynamics | 72 |
| 5.4.3 | Constitutive Equation | 73 |
| 5.5 | Computational Results | 74 |
| 5.6 | Summary | 77 |
| 6 | Nonlinear Feedback Control | 79 |
| 6.1 | Linear Design for a Nonlinear System | 80 |
| 6.2 | Linear Design of Nonlinear SMAs | 82 |
| 6.3 | Summary | 89 |
| 7 | Conclusions | 91 |
| A | Commercial SMAs and Their Applications | 95 |
| A.1 | Commercial Shape Memory Alloys | 95 |

| | | |
|----------|--|------------|
| A.1.1 | Ni-Ti | 96 |
| A.1.2 | Ni-Ti-Cu | 97 |
| A.1.3 | Au-Cu-Zn | 98 |
| A.1.4 | Ni-Mn-Ga | 99 |
| A.1.5 | Thin Film SMAs | 100 |
| A.1.6 | Porous SMAs | 101 |
| A.2 | Shape Memory Alloys Applications | 101 |
| A.2.1 | Medical Applications | 103 |
| A.2.2 | SMAs in Dentistry | 105 |
| A.2.3 | Robotics | 106 |
| A.2.4 | Space Application | 107 |
| A.2.5 | SMA Micro-Damper for Microelectromechanical (MEMS) Ap- plications | 108 |
| B | Maple Routines | 110 |
| B.1 | Numerical simulation | 110 |
| B.2 | Controllability | 111 |
| B.3 | Observability | 112 |
| B.4 | LQR Control | 114 |

List of Tables

| | | |
|-----|---|-----|
| 3.1 | Material Constants of Cu-Zn-Al-Ni SMA in Martensitic Phase [57] . . . | 31 |
| 3.2 | Material Constants of Cu-Zn-Al-Ni SMA in Austenitic Phase [57] . . . | 34 |
| 5.1 | Material Constants of Au-Cu-Zn SMA [77] | 67 |
| A.1 | Ni-Ti Specimens Processed by Spark Plasma Sintering [85] | 102 |
| A.2 | Properties of Different SMAs [48] | 102 |

List of Figures

| | | |
|-----|--|----|
| 2.1 | Types of Stability of an Equilibrium Point | 17 |
| 2.2 | Temperature-induced Phase Transformation of a SMA [30] | 23 |
| 2.3 | Crystal Lattice Deformation of Shape Memory Alloys During SME and Pseudoelasticity [63] | 24 |
| 2.4 | Hysteresis Loop in SMA [73] | 25 |
| 3.1 | One DOF Oscillator | 29 |
| 3.2 | Uncontrolled response of the SMA in its martensitic phase | 32 |
| 3.3 | Phase portrait of the uncontrolled SMA in its martensitic phase | 32 |
| 3.4 | Uncontrolled response of the SMA in its austenitic phase | 35 |
| 3.5 | Portrait of the uncontrolled SMA in its austenitic phase | 35 |
| 4.1 | Controlled and Uncontrolled Response of the Nonlinear Oscillator “Martensitic Phase” | 50 |
| 4.2 | Phase Portrait of the Controlled Nonlinear Oscillator “Martensitic Phase” | 50 |
| 4.3 | Controlled and Uncontrolled Response of the Nonlinear Oscillator “Austenitic Phase” | 54 |

| | | |
|-----|---|-----|
| 4.4 | Phase Portrait of The Controlled Nonlinear Oscillator “Austenitic Phase” | 54 |
| 5.1 | Step Response of SMA During Heating of SMA | 67 |
| 5.2 | Temperature Change During Heating of SMA | 68 |
| 5.3 | Phase Portrait During Heating of SMA | 69 |
| 5.4 | Stress-Strain Curves Illustrating SME and Pseudoelasticity | 69 |
| 5.5 | Strain of SMA during Cooling | 75 |
| 5.6 | Phase transformation of SMA during Cooling | 75 |
| 5.7 | Temperature of SMA during Cooling | 76 |
| 5.8 | Strain versus Temperature of SMA during Cooling | 76 |
| 6.1 | Periodic Orbit: Controlled Response of the Nonlinear Oscillator | 87 |
| 6.2 | Sawtooth: Controlled Response of the Nonlinear Oscillator | 87 |
| 6.3 | Squarewave: Controlled Response of the Nonlinear Oscillator | 88 |
| A.1 | Simon Filter, taken from www.nitinol.com with permission, courtesy of NDC | 103 |
| A.2 | Spinal vertebrae (A) and shape memory spacers (B) in the martensitic state (left) and in the original shape (right). Taken from [37] with permission. | 105 |
| A.3 | Dental Applications of Ni-Ti, taken from http://www.keytometals.com with permission | 106 |
| A.4 | Humanoid Robot Hand [28], taken from http://www.lararobot.de with permission | 107 |
| A.5 | Sketch of the inflatable structure [55] | 108 |

| | |
|--|-----|
| A.6 Prototype of SMA Micro-Damper [61]. Permission granted for non-commercial purposes, courtesy of MDPI (www.mdpi.org). | 109 |
|--|-----|

Chapter 1

Introduction

The interest in intelligent and smart materials has grown in the last decades due to their remarkable properties [50, 53, 56, 65]. This class of materials, usually applied as sensors and actuators in the so called intelligent structures, has the ability of changing its shape and stiffness, among other properties, through the imposition of electrical, electro-magnetic, temperature, or stress fields [50]. Shape memory alloys (SMAs) are a class of this type of materials that are becoming very popular with scientists and researchers, however their inherent nonlinear nature presents a challenge to mathematicians as well as engineers. In this chapter we will look at different constitutive models that describe the behavior of SMAs and the methods that have been used to solve these models. Also, some historical notes accounting for the developments of SMAs are given.

1.1 Shape Memory Alloys

SMA s are typically metallic alloys that have the ability to recover a previously defined shape when subjected to the appropriate thermal procedure. Generally, these materials can be deformed at some relatively low temperature, and when they are heated they return to their shape prior to deformation. The shape recovery occurs even under applied loads therefore resulting in high actuation energy densities. In addition, under specific conditions, SMA s can absorb and dissipate mechanical energy by undergoing a reversible hysteretic phase change when subjected to applied mechanical cyclic loading [30]. SMA s present complex thermo-mechanical behaviors related to different physical processes, and the most common phenomena presented by this class of materials, are pseudoelasticity, shape memory effect (SME), and phase transformation due to temperature variation [53] ¹. Due to these unique characteristics of SMA s, materials made of SMA s lend themselves to be used in many innovative applications in many scientific fields for sensing and actuation, ranging from biomedical devices, such as stents , prosthetic limbs, and orthodontics, to apparatus for the deployment and control of space structures, such as antennas and satellites ². SMA s have also been used in vibration control devices to improve the response of buildings and bridges subjected to seismic loads [18, 73]. In order to explore all potentials of SMA s, there has been an increasing interest in the development of mathematical models capable of describing the main behaviors of these alloys. In the next section we will explore some of these models.

¹Further details about the properties of SMA s will be given in Chapter 2

²For commercial SMA s and their applications see Appendix A

1.2 Overview of Constitutive Models for SMAs

Over the years a great deal of research has been carried out in the study of complex thermo-mechanical response of shape memory alloys, many researchers have proposed a variety of constitutive models with the goal to predict the behavior of such materials. This section presents a summary of some of these models, and for further details on these and related models, one can consult [6, 18, 30, 53].

1.2.1 The Polynomial Model

One of the most popular constitutive models for describing the behavior of SMAs stems from the original Landau-Ginzburg theory of phase transitions in systems such as ferroelectric and ferromagnets [16]. In [15], the author proposed a one-dimensional model based on Devonshire's generalization of the theory. This model assumes a polynomial free energy potential, which allows pseudoelasticity and SME description. According to this model, neither internal variables nor dissipation potential is necessary to describe pseudoelasticity and SME. Thus, the only state variables for this model are strain and temperature. The form of the free energy is chosen in such a way that the minima and the maxima points present stability and instability of each phase of the SMA. Hence, the free energy is chosen such that for high temperatures, it has only one minimum at vanishing strain, representing the equilibrium of the austenitic phase. At low temperatures, martensite is stable, and the free energy must have two minima at non-vanishing strains. At intermediate temperatures, the free energy must have equilibrium points corresponding to both phases. Therefore, the free energy is defined as a sixth-order polynomial equation in a way that the minima and maxima

points represent stability and instability of each phase of the SMA. Three phases are considered: austenite (A) and two variants of martensite ($M+$, $M-$). Hence, the form of the free energy is chosen such that for high temperatures ($T > T_A$), it has only one minimum at vanishing strain, representing the equilibrium of the austenitic phase. For intermediate temperatures ($T_M < T < T_A$), there are three minima corresponding to three stable phases: austenite, and detwinned martensite induced by tension ($M+$) and by compression ($M-$). Lastly, at low temperatures ($T < T_M$), martensite is stable, and the free energy must have two minima at nonvanishing strains [53, 57]. Therefore, the following free energy potential is defined as:

$$W(\epsilon, T) = \frac{a}{2}(T - T_M)\epsilon^2 - \frac{1}{4}b\epsilon^4 + \frac{b^2\epsilon^6}{24a(T_A - T_M)}, \quad (1.1)$$

where a and b are positive material constants, T_A is the temperature above which austenite is stable and T_M is the temperature below which martensite is stable. Thus, the constitutive equation is given by:

$$\sigma(\epsilon, T) = \frac{\partial}{\partial \epsilon} W(\epsilon, T) = a(T - T_M)\epsilon - b\epsilon^3 + \frac{b^2\epsilon^5}{4a(T_A - T_M)}. \quad (1.2)$$

The great advantage of this model, also known as Falk's model, bearing the name of its inventor, is its simplicity [53].

1.2.2 The Exponential Model

The exponential model, also known as the Tanaka model, considers, besides strain and temperature, an internal variable used to represent the phase transformation when the SMA changes from the martensitic phase to the austenitic phase [18, 30, 53]. The constitutive relation between stress, temperature, and the phase transformation

variable for SMA modeling is considered in the rate form as follows:

$$\dot{\sigma} = E\dot{\epsilon} + \alpha\dot{\zeta} + \Gamma\dot{T}, \quad (1.3)$$

where E represents the elastic tensor, α corresponds to the phase transformation tensor, and Γ is associated with the thermo-elastic tensor. Due to martensitic transformation non-diffusive nature, the martensitic volumetric fraction, ζ , can be expressed as a function of current values of stress and temperature $\zeta = \zeta(\sigma, T)$. For example, in [70], the authors considered exponential functions to describe phase transformations. Following that idea, for ($A \implies M$) transformation, we can consider the following function:

$$\zeta = 1 - \exp [a_M (M_s - T) - b_M \sigma] + \zeta_0, \quad (1.4)$$

where a_M and b_M are positive material parameters, M_s is the martensite formation start temperature, T is temperature, and ζ_0 represents the volumetric fraction when phase transformation takes place.

For the reverse transformation ($M \implies A$) another exponential function is considered as follows:

$$\zeta = \zeta_0 \exp [-a_A (T - A_s) - b_A \sigma], \quad (1.5)$$

where a_A and b_A are positive material constants and A_s is the austenite formation start temperature.

1.2.3 The Trigonometric Model

Other functional dependencies for constitutive models are also used. In [35] for instance, the authors developed an empirical cosine model, to represent the martensitic

fraction as a function of stress and temperature during transformation, which agrees well with experimental findings [5]. According to this model, the volumetric fraction evolution equation for the martensitic transformation ($A \implies M$) is given by:

$$\zeta = \frac{(1 - \zeta_0)}{2} \cos \left[A_M \left(T - M_f - \frac{\sigma}{C_M} \right) \right] + \frac{(1 + \zeta_0)}{2}, \quad (1.6)$$

where T is temperature, σ is stress, C_M is a material parameter, and M_f and M_s correspond to the martensite formation finish and start temperature, ζ_0 represents the volumetric fraction of the material prior to the current transformation, and the coefficient A_M is defined in terms of M_f and M_s and is given by:

$$A_M = \frac{\pi}{M_s - M_f}. \quad (1.7)$$

For the reverse transformation ($M \implies A$), the equation is given by:

$$\zeta = \frac{\zeta_0}{2} \left[\cos \left(A_A \left(T - A_s - \frac{\sigma}{C_A} \right) \right) + 1 \right], \quad (1.8)$$

where C_A is a material parameter, A_s and A_f represent the austenite formation start and finish temperatures, and A_A is defined in terms of A_f and A_s and is given by:

$$A_A = \frac{\pi}{A_f - A_s}. \quad (1.9)$$

1.2.4 The Model Based on the Fermi-Dirac Statistics

Since a SMA exists only in martensite and austenite phases, it can be modeled as a two-state system, like an electron. The Fermi-Dirac statistics, which describes the distribution of electrons in two states depending on their energy levels, has been found to provide a good model for the state of an SMA in martensite and austenite

forms [24]. Since the SMA is in the martensite form at lower temperatures, the phase transformation equation during heating is described by analogy with the Fermi-Dirac statistics in the form:

$$\zeta = \frac{\zeta_m}{1 + \exp \left[\frac{T_{fa} - T}{\sigma_a} + K_a \sigma \right]}, \quad (1.10)$$

where ζ is the fraction of the austenite phase, ζ_m is the fraction of the martensite phase prior to the present transformation from martensite to austenite, T is the temperature, T_{fa} is the transition temperature from martensite to austenite, σ_a is an indication of the range of temperature around the transition temperature T_{fa} during which the phase change occurs, σ is the stress, and K_a is the stress curve-fitting parameter which is obtained from the stress-strain characteristic with no change in temperature. On cooling, the austenite phase gets converted to the martensite phase and the modeling equation during cooling is described by analogy with the Fermi-Dirac statistics in the form:

$$\zeta = \frac{\zeta_a}{1 + \exp \left[\frac{T_{fm} - T}{\sigma_m} + K_m \sigma \right]}, \quad (1.11)$$

where ζ_a is the fraction of the austenite phase prior to the transformation from austenite to martensite, T is the temperature, T_{fm} is the transition temperature from austenite to martensite, σ_m is an indication of the range of temperature around the transition temperature T_{fm} during which the phase change occurs, σ is the stress, K_m and is the stress curve-fitting parameter which is obtained from the stress-strain characteristic. Since the SMA is modeled as a two-component system, at any given time the sum of the mole fractions of the austenite and martensite phase is 1, *i.e.*,

$$\zeta_a + \zeta_m = 1. \quad (1.12)$$

The time derivatives of (1.10) and (1.11) are as follows:

- for heating

$$\frac{d}{dt}\zeta = \frac{\zeta^2}{\zeta_m} \exp \left[\frac{T_{fa} - T}{\sigma_a} + K_a \sigma \right] \left(\frac{1}{\sigma_a} \frac{d}{dt} T - K_a \frac{d}{dt} \sigma \right), \quad (1.13)$$

- for cooling

$$\frac{d}{dt}\zeta = \frac{\zeta^2}{\zeta_a} \exp \left[\frac{T_M - T}{\sigma_m} + K_m \sigma \right] \left(\frac{1}{\sigma_m} \frac{d}{dt} T - K_m \frac{d}{dt} \sigma \right). \quad (1.14)$$

1.2.5 The Fremond Model

The Fremond model is another constitutive model that describes the thermo-mechanical behavior of SMAs. The proposed model formulation considers four volumetric fractions related to macroscopic phases: β_1 is associated with tensile detwinned martensite ($M+$), β_2 is related to compressive detwinned martensite ($M-$), β_3 represents austenite (A) and β_4 corresponds to twinned martensite (M). A Helmholtz free energy potential (ψ) is adopted for each individual phase, considering four state variables: elastic strain (ϵ), temperature (T) and two internal variables (γ and μ) that help the plastic phenomenon description, which are associated with the isotropic and kinematic hardening, respectively [67]. The constitutive thermo-mechanical model of SMAs is then given by:

$$M+ : \rho \psi_1 (\epsilon, T, \gamma, \mu) = \frac{1}{2} E_M \epsilon^2 - \alpha^T \epsilon - \Lambda_M^T - \Omega_M (T - T_0) \epsilon + \frac{1}{2} K_M \gamma^2 + \frac{1}{2 H_M} \mu^2, \quad (1.15)$$

$$M- : \rho \psi_2 (\epsilon, T, \gamma, \mu) = \frac{1}{2} E_M \epsilon^2 + \alpha^C \epsilon - \Lambda_C^T - \Omega_M (T - T_0) \epsilon + \frac{1}{2} K_M \gamma^2 + \frac{1}{2 H_M} \mu^2, \quad (1.16)$$

$$A : \rho \psi_3(\epsilon, T, \gamma, \mu) = \frac{1}{2} E_A \epsilon^2 - \Lambda_A - \Omega_A (T - T_0) \epsilon + \frac{1}{2} K_A \gamma^2 + \frac{1}{2 H_A} \mu^2, \quad (1.17)$$

$$M : \rho \psi_4(\epsilon_e, T, \gamma, \mu) = \frac{1}{2} E_M \epsilon_e^2 - \Lambda_M - \Omega_A (T - T_0) \epsilon + \frac{1}{2} K_M \gamma^2 + \frac{1}{2 H_M} \mu^2. \quad (1.18)$$

In equations (1.15)-(1.18), subscript M is related to martensitic phase while A is associated with austenite. Moreover, superscript T is related to tensile parameters while C is associated with compressive parameters. Observing these indices, notice that α 's are material parameters related to phase transformation, while Λ 's are associated with phase transformations stress levels and are temperature dependent, while E 's represent the elastic moduli, Ω 's are related to the thermal expansion coefficients, K 's are the plastic modulus while H 's are the kinematic hardening moduli; T_0 is a reference temperature, ψ_i for $i = 1..4$ are the free energy potentials corresponding to the phases ($M+$), ($M-$), (A), and (M), and ρ is the material's density.

1.3 Numerical Implementations

The constitutive models discussed in section 1.2 are amongst the models that are widely used in describing the behavior of SMAs. These models combined with the dynamic equations of SMA systems form the basis of the mathematical models that describe their dynamic characteristics. A common feature of SMAs is the presence of hysteresis, which causes the input-output relations to be nonlinear. Because of the nonlinearities associated with the hysteresis, and the complex thermo-mechanical coupling of SMAs, the dynamic equations of SMAs are usually represented by complex systems of PDEs or ODEs that do not have analytic solutions. Therefore, a number of approximation methods have been implemented to solve these type of systems of equations. Some common methods have been used by a number of authors

including, finite element analysis (FEA) [6], finite volume analysis (FVA) [77] and model reductions [43, 52, 75]. Since we are interested in using the SMA as an actuator to pull mass m of the oscillator shown in Figure 3.1, the polynomial constitutive model discussed in section 1.2.1 will be used as it is capable of describing the shape memory effect of the SMA that produces the actuation. In Chapter 3, we will use the polynomial constitutive model to develop a mathematical model of the one degree of freedom (1 DOF) oscillator with a SMA at constant temperature. The model will then be solved numerically and results will be presented. In chapter 5 we will develop a thermo-mechanical model for the nonlinear oscillator with a SMA, but due to the complexity of the model, model reduction method based on Galerkin decomposition will be used to transform the model into a system of ODEs.

1.4 Historical Notes

In 1932, a Swedish physicist by the name of Arne Ölander discovered an interesting phenomenon when working with an alloy of gold (Au) and cadmium (Cd) [32]. The Au-Cd alloy could be plastically deformed when it is cool and then be heated to return to, or “remember”, the original dimensional configuration. This phenomenon is known as the shape memory effect “SME”, and the alloys that exhibit the behavior are called shape memory alloys. In 1958, shape memory effect was demonstrated at the Brussels World’s Fair, where the SME was used to cyclically lift a load mass using a Au-Cd SMA [48]. Further research revealed other materials that demonstrate this phenomenon. In 1961, a group of U.S. Naval Ordnance Laboratory researchers led by William Beuhler came across a significant discovery in the field of SME and SMA

[50]. While testing an alloy of nickel and titanium for heat and corrosion resistance, they found that it too exhibited the shape memory effect. The Ni-Ti shape memory alloy proved to be significantly less expensive, easier to work with than previously discovered alloys. These factors refreshed interest and research in the shape memory effect and its applications.

Researchers, designers, and companies recognized the potential to use the shape memory effect in engineering, biomedical, and scientific applications. As a result, starting in the 1970s, commercial products began to appear. For the most part, the early devices functioned as fasteners and took advantage of a single shape memory dimensional change. Some examples of these static devices are couplings for piping systems and electrical connectors. Next, researchers began to propose SMA devices to perform dynamic tasks; thus, they began to play the role of actuators. In order to perform a dynamic task, the SMA must experience a cycle of heating, cooling, and deformation. This requirement led some companies, such as Delta Metal in England, to use shape memory alloy actuators in temperature regulation systems, where the environmental temperature could be used for thermal actuation [40]. Delta Metal proposed that SMA devices could be used to automatically open and close greenhouse windows, operate valves that control building temperatures, and control automobile fan clutches. In 1982 Sharp incorporated SMA actuators into electric oven dampers, and in 1983 Matsushita Electric [32] designed SMA-actuated louvers for air conditioners. Other researchers pursued electricity as a source of heat and thus actuation. In 1971, a team led by Sawyer developed and tested an artificial heart powered by electrical actuation of SMA elements. In 1983, Honma, Miwa, and Iguchi showed that SMA actuation could be controlled by resistive heating and proposed that SMA actuators

could be used in micro-robotics. Research concerning the application and control of SMA actuators in robotic systems has continued and expanded through the present [53]. While design, modeling and dynamics of SMAs have been studied extensively, very little work has been done in the area of control [32, 57]. In this thesis we will address the issue of modeling and control of an SMA device using the laws of physics and optimal control techniques.

1.5 Thesis Outline

This thesis is organized in 6 chapters, conclusions, and appendices as follows:

In Chapter 2 we will give an overview of dissipative systems, dissipative systems in an Input/State/Output setting, and the general properties of SMAs.

In Chapter 3 a mathematical model of a nonlinear oscillator with a SMA device is developed. The model is then simulated for each of the two separate phases of the SMA, the martensitic phase and austenitic phase.

Chapter 4 is devoted to the optimal control of the nonlinear 1 DOF oscillator.

The hysteresis phenomenon in SMAs results in a nonlinear relationship between the input and output of the 1 DOF oscillator system. To compensate for the hysteresis phenomenon, Lyapunov indirect method will be used to design a Linear Quadratic Regulator controller to stabilize the system while at the same time optimize a certain performance measure.

In Chapter 5 a thermo-mechanical model that accounts for the effect of temperature on the SMA will be developed, and model reduction, using Galerkin's method, will

be used to transform the system into a low-dimensional one. In Chapter 6 a nonlinear feedback control method will be used to design a nonlinear controller of the SMA. Numerical methods will then be used to find an approximate solution of the controlled model. In Chapter 7 we will give a summary of what was achieved in this research and we will conclude highlighting future directions.

1.6 Summary

The work presented in this thesis accomplished a number of results in terms of modeling and control of the SMA. In Chapter 4 for example, the nonlinear model of the SMA oscillator was linearized and a Linear Quadratic Regulator (LQR) controller was designed and implemented to control and stabilize its response. In Chapter 5, a thermo-mechanical model that accounts for the effect of temperature on the response of the nonlinear oscillator with a SMA was modeled by a single nonlinear ODE. This result was achieved by applying a model reduction based on the Galerkin method to transform the mathematical model describing the behavior of the SMA system into an approximate, low dimensional one. Numerical results show that the model does capture the main properties of the SMA, mainly shape memory and superelasticity properties. In Chapter 6, an optimal linear control design for nonlinear systems strategy was implemented to compensate for the hysteresis phenomenon of SMAs and to track the response of the SMA to a desired trajectory. A number of examples are included at the end of Chapter 6 that showed the effectiveness of the proposed method. All the simulation results were obtained by using Maple's routines and algorithms

summarized in Appendix B.

Chapter 2

Dissipative Systems and General Properties of Shape Memory

Alloys

Dissipation is a physical concept closely related to the first and the second law of thermodynamics. Recall that the first law ensures conservation of mass and energy in all its forms, while the second law determines the way in which the different forms of energy and material species evolve through transport phenomena and chemical reactions, taking place in a given spatial domain [1]. Shape memory alloys are dissipative systems, therefore it is essential that we first give a brief overview of dissipative systems and how they relate to shape memory alloys.

2.1 Dissipative Systems

Dissipativity theory gives a framework for the design and analysis of control systems using an input-output description based on energy-related considerations. Dissipativity is a notion which can be used in many areas of science, and it allows engineers and mathematicians to relate a set of efficient mathematical tools to well known physical phenomena [7]. The dissipation hypothesis on dynamical systems results in a fundamental constraint on their dynamic behavior, wherein a dissipative dynamical system can deliver only a fraction of its energy to its surroundings and can store only a fraction of the work done to it [22]. In this context, dissipation imposes a particular relationship between transport processes and their associated thermodynamic forces which guide the dynamic evolution of the system, giving room to variety of complex behaviors, such as hysteresis in the case of shape memory alloys. The constraints imposed on the dynamic behavior of dissipative systems actually present a challenge to both engineers and mathematicians, and a great deal of research has been done in this area. In this thesis optimal nonlinear control methods combined with Lyapunov stability methods will be used to deal with the constraints imposed on the dynamic behavior of shape memory alloys. The dissipativity theory for non-linear dynamical systems has been developed by many authors (see, e.g., [71, 72] and references therein). Based on this theory, the definition of dissipativity for general non-linear dynamical systems can be formulated in terms of a dissipation inequality involving a generalized system power input, or supply rate, and a generalized energy function, or storage function. The dissipation inequality implies that the increase in generalized system energy over a given time interval cannot exceed the generalized energy supply

delivered to the system during this time interval. The set of all possible system storage functions is convex and every system storage function is bounded from below by the available system storage and bounded from above by the required energy supply [22].

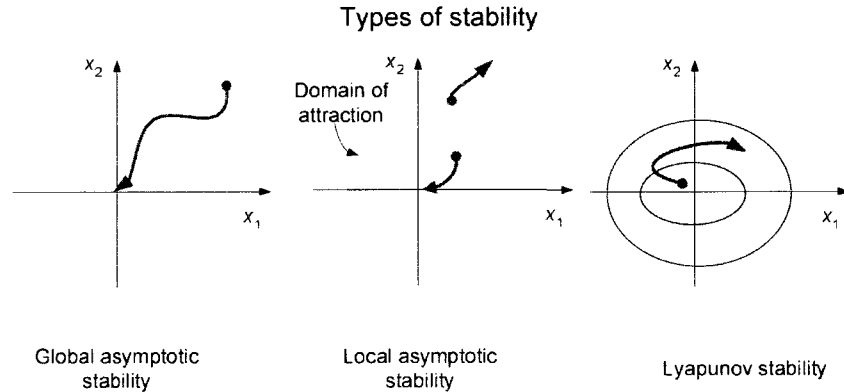


Figure 2.1: Types of Stability of an Equilibrium Point

The connections between input, output and state space stability for nonlinear systems have been established by the theory of dissipativity in which a Lyapunov-like storage function is used to monitor the “energy” flowing in and out of a system [17].

Stability theory plays an important role in engineering, physical as well as biological, systems. For any given dynamic system, stability is crucial, since unstable systems can oscillate uncontrollably and could lead to system failure. There are different kinds of stability problems that arise in the study of dynamic systems, but in the first part of this thesis we will focus on the stability of the 1 DOF oscillator in the vicinity of a stable equilibrium point, and in the second part we will use tracking control theory to make the system track a given reference input signal. Stability of equilibrium points,

see Figure 2.1, is usually characterized in the sense of Lyapunov¹ stability theory, which includes two methods, Lyapunov's first method and Lyapunov's direct method, also known as the second method [25].

In Chapter 4 Lyapunov's first method which uses the idea of system linearization around a given equilibrium point will be used to design a linear quadratic regulator (LQR) to control the response of the shape memory alloy. Since the linearized model may drastically reduce the stability region of the nonlinear system, in Chapter 6 a nonlinear feedback control method will be used to design a tracking controller to achieve global stability. The basic concept behind Lyapunov's direct method is that if the total energy of the system is continuously dissipating, then the system will eventually reach an equilibrium point and remain at that point. In general, Lyapunov's direct method includes two steps, first find a scalar function, referred to as Lyapunov function, second evaluate its first time derivative along the trajectory of the system. If the Lyapunov function derivative is decreasing along the system's trajectory as time increases, then the system's energy is dissipating and thus the system will eventually settle down [17].

2.2 Dissipative Systems in an Input/State/Output Setting

In "closed" dynamical systems the response of the system is determined by the initial conditions. The trajectory is autonomous and driven purely by the internal dynamics

¹A Russian mathematician and engineer who laid the foundation of the theory which now carries his name

of the system, the environment has no influence on the motion. On the other hand “open” dynamical systems, take the influence of the environment explicitly into consideration. They are a much more logical and richer starting point for a theory of dynamics leading to the concept of generalized dynamic systems[41, 42]. In the state space models of systems and control this interaction with the environment can be formalized through inputs and outputs. The environment acts on the system by imposing inputs, and the system reacts through the outputs [82]. This leads to models of the form:

$$\dot{x} = f(x, u), \quad y = h(x, u) \quad (2.1)$$

with u the input value, U the input space, $u \in U$, y the output value, Y the output space, $y \in Y$, and x the state, X the state space, $x \in X$. The map f is called the controlled vector field, and h is called the read-outs. Thus the vector field assigns to $(x, u) \in X \times U$ the state “velocity” $\dot{x} = f(x, u)$, and the read-out assigns to $(x, u) \in X \times U$, the output value $y = h(x, u) \in Y$. The notion of dissipative systems involves:

- a dynamical system Σ in the form of equation (2.1),
- a real-valued function: $s : U \times Y \rightarrow \mathbb{R}$ called the supply rate, and
- a real-valued function $V : X \rightarrow \mathbb{R}$, called the storage.

Definition 1 [82]: *The system Σ is said to satisfy the dissipation inequality with respect to the supply rate s and the storage V if*

$$V(x(t_2)) - V(x(t_1)) \leq \int_{t_1}^{t_2} s(u, y) dt \quad (2.2)$$

holds for all (u, y, x) and $t_1, t_2 \in \mathbb{R}$, with $t_1 \leq t_2$, The above inequality (2.2) is known as *Dissipation Inequality*.

In the case of Lyapunov function, the dissipation inequality can be verified directly from the vectorfield f , the supply rate s , and the storage V .

Then, the dissipation inequality holds if and only if:

$$\dot{V} = \Delta V f \tag{2.3}$$

satisfies

$$\dot{V} \leq s(u, h(x, u)) \tag{2.4}$$

for all $x \in X$ and $u \in U$.

Definition 2 [82]: Consider the dynamic Σ , the function $V : X \rightarrow \mathbb{R}$ is said to be *Lyapunov for Σ along $x \in X$ if:*

$$\frac{d}{dx} V(x) \leq 0. \tag{2.5}$$

The system Σ is said to be *dissipative with respect to the supply rate $s : U \times Y \rightarrow \mathbb{R}$ if there exists a Lyapunov function $V : X \rightarrow \mathbb{R}$ such that the dissipation inequality (2.2) holds. In the linear-quadratic case, the system is assumed to be linear, and the supply rate a quadratic in (u, x) .*

Theorem 1 [25] (*Lyapunov stability for autonomous systems*): Let x^* be an equilibrium point for Σ and $X \in \mathbb{R}$ be a domain containing x^* . Let $V : X \rightarrow \mathbb{R}$ be a Lyapunov function, such that $V(0) = 0$ and $V(x) \geq 0$ in $X - \{0\}$. If $V(x) \leq 0$ in X , then, x^* is stable. Moreover, if $V(x) < 0$ in $X - \{0\}$ then x^* is asymptotically stable.

The concept of dissipativity is closely connected to the stability and control of dynamic systems [21, 22, 71, 72]. In dissipative systems the storage function is usually chosen as a Lyapunov function, and thus the stability of dissipative systems can be investigated [83]. Since SMAs are dissipative systems, the concept of dissipativity and Lyapunov stability will be used in Chapter 4 to design a controller in order to stabilize a nonlinear 1 DOF nonlinear oscillator with and SMA device.

2.3 General Properties of SMAs

In section 2.2 we looked at dissipativity and stability of dynamic systems. In this section we will look at the general properties of SMAs that are used as actuators or transducers which are often found in many dynamic systems. We have seen in section 1.1 of Chapter 1 that when SMAs are subjected to thermal procedures they go through phase transformations that cause the SMA to change its crystalline structure. The change in the crystal structure of SMAs is associated with two main phases, austenite and martensite. At high temperature the SMA is in the austenitic phase, and at low temperature the SMA is in the martensitic phase. Austenite (generally cubic) has a different crystal structure from martensite (tetragonal, orthorhombic or monoclinic), see Figure 2.3. Martensite is relatively soft, whereas austenite is relatively hard [40]. The phase transition from austenite to martensite is termed the forward transformation. When the SMA is heated from the martensitic phase, the crystal structure transforms back to austenite, and this transition is called reverse transformation, during which there is no associated shape change. The phase transformation from martensite (product phase) to austenite (parent phase) and vice versa

forms the basis for the unique behavior of SMAs.

There are four characteristic temperatures associated with the phase transformation. During the forward transformation, austenite, under zero load, begins to transform to twinned martensite at the martensitic start temperature M_s and completes transformation to martensite at the martensitic finish temperature M_f , see Figure 2.2. At this stage, the transformation is complete and the material is fully in the twinned martensitic phase. Similarly, during heating, the reverse transformation initiates at the austenitic start temperature A_s and the transformation is completed at the austenitic finish temperature A_f . If a mechanical load is applied to the material in the twinned martensitic phase (at low temperature), a subsequent heating of the SMA to a temperature above A_f will result in a reverse phase transformation (from martensite to austenite) and will lead to complete shape recovery. Cooling back to a temperature below M_f (forward transformation) leads to the formation of twinned martensite again with no associated shape change observed. The process described above is referred to as the Shape Memory Effect (SME), which was mentioned in section 1.1 of Chapter 1. In addition to thermally induced phase transformation, transformation can also be induced by applying a sufficiently high mechanical load to the material in the austenitic phase. The result of this load is fully detwinned martensite created from austenite. If the temperature of the material is above A_f , a complete shape recovery is observed upon unloading to austenite. This material behavior is called the pseudoelastic effect [30]. Pseudoelasticity and SME are some of the properties that make SMAs so unique an appealing to lot of researchers and scientists. In sections 2.3.1 and 2.3.2 we will further explore the shape memory effect and the pseudoelasticity of SMAs and how they impact the response of SMA

dynamical systems.

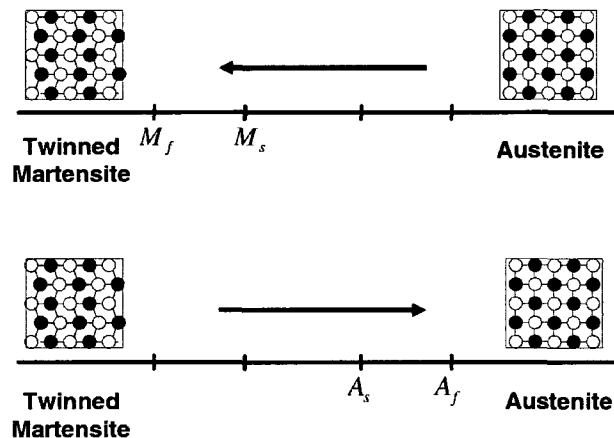


Figure 2.2: Temperature-induced Phase Transformation of a SMA [30]

2.3.1 Shape memory effect

Since SMAs are stimuli-responsive materials, they have the capability of changing their shape upon application of an external stimulus. A SMA exhibits the shape memory effect when it is deformed while in the martensitic phase and then unloaded while at a temperature below A_s . When it is subsequently heated above A_f , the SMA will regain its original shape by transforming back into the parent austenitic phase. A change in shape caused by a change in temperature is called a thermally induced shape-memory effect. In order to understand this phenomenon (SME), it is useful to consider the highly simplified representation of the material's crystalline arrangement shown in Figure 2.3. In the martensitic phase the molecular structure is twinned, which is the configuration shown in the middle of Figure 2.3. Upon

deformation this phase takes on the second form shown in Figure 2.3, on the right. Austenite, the stronger phase of shape memory alloys, occurs at higher temperatures. The shape of the austenitic structure is cubic, the structure shown on the left side of Figure 2.3. The undeformed martensite phase is the same size and shape as the cubic austenitic phase on a macroscopic scale, so that no change in size or shape is visible in shape memory alloys until the martensite is deformed [38]. The change that occurs within a SMA crystalline structure during the SME is not a thermodynamically reversible process. In other words, there is energy dissipation due to internal friction and creation of structural defects. As a result, a temperature hysteresis occurs which is illustrated in Figure 2.4.

In Figure 2.4 M_t is the temperature below which the martensitic phase is stable and A_t is the temperature above which the austenitic phase is stable . The crystalline structure is in its deformable phase (martensite) when its temperature is lower than

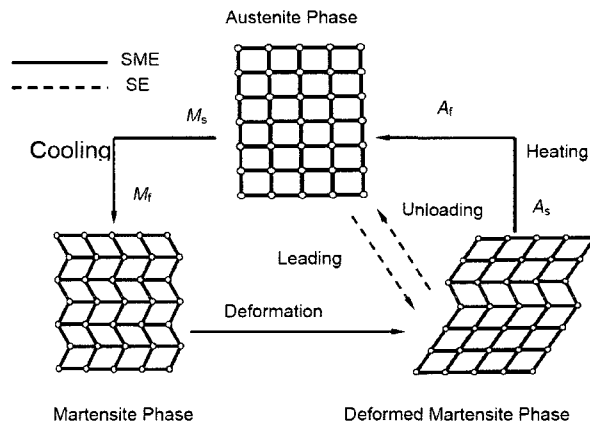


Figure 2.3: Crystal Lattice Deformation of Shape Memory Alloys During SME and Pseudoelasticity [63]

the M_t . In this state the SMA length can be changed about 10% as a consequence of external stress. If the material is heated to temperature A_t (line 1 in Figure 2.4) the crystalline structure will change to hard non-deformable state (austenite). If the temperature is held at A_t the element of the SMA stay in contracted state (line 3 Figure 2.4). When the temperature is increased over point A_t , the shape memory effect (SME) of the material can be completely destroyed. It means that the material loses SME (element will stay contracted forever) [73].

2.3.2 Superelasticity of SMAs

Superelasticity, or pseudoelasticity, occurs whenever a SMA sample is at a temperature above A_t (the temperature above which only the austenitic phase is stable for a stress-free specimen). Thus, one can consider a SMA sample subjected to a mechanical loading at a constant temperature above A_t . A mechanical loading causes an elastic response until a critical value is reached, when the martensitic transformation

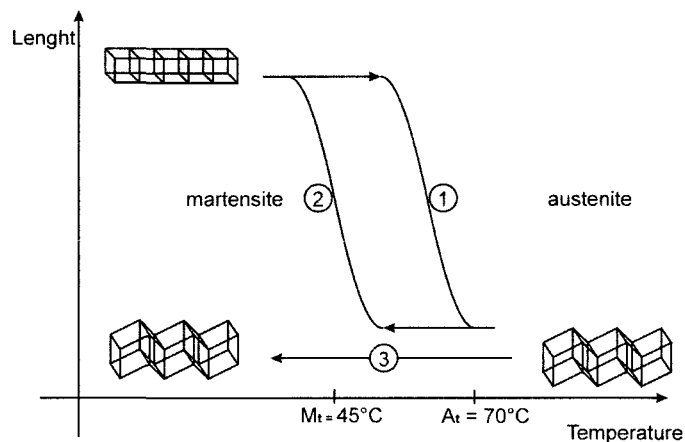


Figure 2.4: Hysteresis Loop in SMA [73]

(austenite to martensite) arises. At this point, the crystal structure of the sample is totally composed of detwinned martensite. For higher stress values, SMA presents a linear response. During the unloading process, the sample presents an elastic recovery. When the loading-unloading process is finished, SMA has no residual strain. However, since the path of the forward martensitic transformation does not coincide with the reverse transformation path, there is a hysteresis loop associated with energy dissipation as was seen in Figure 2.4 [37]. In Chapter 3, we will utilize the shape memory effect of SMAs to model a 1 DOF nonlinear oscillator. The 1 DOF model consists of a mass connected to a fixed frame through a viscous damping and a SMA device in the form of a nonlinear spring. When the SMA spring is heated, it will exert a restoring force on mass m of the oscillator. Since the SMA exists in two phases, martensitic and austenitic, two models will be developed and analyzed by choosing a temperature where the SMA exists in a single phase.

2.4 Summary

In this chapter we discussed the concept of dissipativity and how it is related to the stability of dynamic systems. We also gave an overview of the general properties of SMAs that make them a hot topic in so many areas of scientific research. SMAs, as we have seen in section 2.3, have unique characteristics, especially the shape memory effect that makes them suitable for use as actuators. It is this unique property, the shape memory effect, that we will use to develop and analyze a 1 DOF nonlinear oscillator with a SMA device acting as an actuator. The concept of dissipativity and stability will be used in Chapter 4 to overcome the hysteresis phenomenon of SMAs

and to stabilize their response.

Chapter 3

Mathematical Modeling of Nonlinear Oscillators with Shape Memory Alloys at Constant Temperature

Developing a mathematical model that captures the behaviors of a SMA as it undergoes temperature, stress, and phase changes is a complicated and challenging problem. Researchers continue to study what are the best ways to model and control systems that use this unique family of materials [40].

Over the years researchers have proposed a number of constitutive models with the objective of predicting the dynamical behavior of shape memory alloys, and different models were discussed in Chapter 1. In this chapter a mathematical model of the shape memory alloy is formulated based on the polynomial constitutive model, and

then a 1 DOF nonlinear oscillator with a SMA device is used to analyze and simulate its response. We will consider the system only when it exists in one of its two different phases, martensite and austenite, and to achieve this the temperature will be chosen in such a way that only one of the phases is stable.

3.1 Mathematical Model of a Nonlinear Oscillator with a SMA

To study the behavior of the SMA we will consider a one degree of freedom oscillator which consists of mass m , connected to a rigid support through of a viscous damping with coefficient c and a shape memory alloy element in the form of a nonlinear spring where a periodic external force $u(t)$ is applied to the system, as shown in Figure 3.1.

In Figure 3.1 the SMA is represented by a nonlinear spring K that will exert a

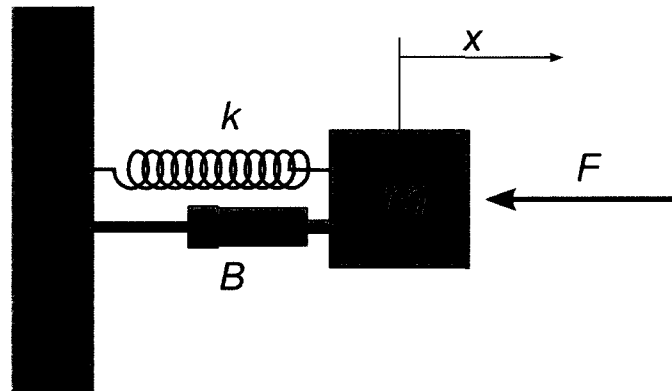


Figure 3.1: One DOF Oscillator

restoring force on mass m . To be specific, in our analysis and computations that follow

we use all values for a spring made of Cu-Zn-Al-Ni alloy. The behavior of the nonlinear spring with shape memory is described by the polynomial constitutive model given in equation (1.2). Therefore, the restoring force is determined by substituting (ϵ) by the displacement $x(t)$ of mass m in equation (3.1):

$$K(x, T) = a(T - T_M)x(t) - bx(t)^3 + \frac{b^2x(t)^5}{4a(T_A - T_M)}. \quad (3.1)$$

Using Newton's law of dynamics, the dynamic equation of the system in Figure 3.1 is given by:

$$m \frac{d^2}{dt^2}x(t) + c \frac{d}{dt}x(t) + a(T - T_M)x(t) - b(x(t))^3 + \frac{b^2(x(t))^5}{4a(T_A - T_M)} = u(t), \quad (3.2)$$

where $x(t)$ is the displacement and $u(t)$ is the input representing the external force. The different phases of the SMA system are defined by the choice of the temperature T [57], therefore we will study the system given by equation (3.2) while the SMA is in its two different phases, austenitic and martensitic. In sections 3.2 and 3.3 we will study the behavior of the SMA system by carefully choosing the temperature T and the parameters a , b , T_A and T_M of the SMA element, keeping in mind that at high temperatures the austenitic phase of the SMA is stable, and at low temperature the martensitic phase of the SMA is stable.

3.2 Analysis of the Martensitic Phase

For a temperature $T \leq T_M$, where T_M is the temperature below which the martensitic phase of the SMA is stable, the SMA is in its martensitic phase. The numerical values of the SMA parameters, a , b , T_M , and T_A that will be used in the analysis are given in Table 3.1 [57], and we choose a temperature $T = 283K$ so that the

Table 3.1: Material Constants of Cu-Zn-Al-Ni SMA in Martensitic Phase [57]

| Parameters | Values |
|------------|----------------------|
| a | 1 MPa |
| b | 40×10^3 MPa |
| T_M | 287 K |
| T_A | 364 K |
| T | 283 K |

SMA is in its martensitic phase. The first numerical experiment deals with the SMA at low temperatures, or more precisely when the SMA is in its martensitic phase. Substituting the parameters a, b, T_M , T_A , and T given in Table 3.1 in the dynamic equation (3.2), and choosing as a mechanical load a time-varying periodic input force $u(t) = 10 \sin(5t)$, we get a second order nonlinear differential equation that represents the SMA in its martensitic phase:

$$\frac{d^2}{dt^2}x(t) + 0.2 \frac{d}{dt}x(t) - 4x(t) - 40000.0x(t)^3 + 5194805.195x(t)^5 = 10 \sin(5t). \quad (3.3)$$

We will assume a unit mass and the following initial conditions $x(0) = 0.1$ and $x'(0) = 0$. We now have a nonlinear ordinary differential equation in $x(t)$, where $x(t)$ is the displacement of mass m, and t is the time variable. The numerical results shown in Figures 3.2 and 3.3 were obtained using Maple's Runge-Kutta-Fehlberg method (*RKF45*) for solving ordinary differential equations.¹

From the numerical analysis (see Figures 3.2 and 3.3) that was performed on the model given by equation 3.2, we observed that the response of the 1 DOF oscillator

¹The Maple code used to solve the nonlinear differential equation is given in Appendix B

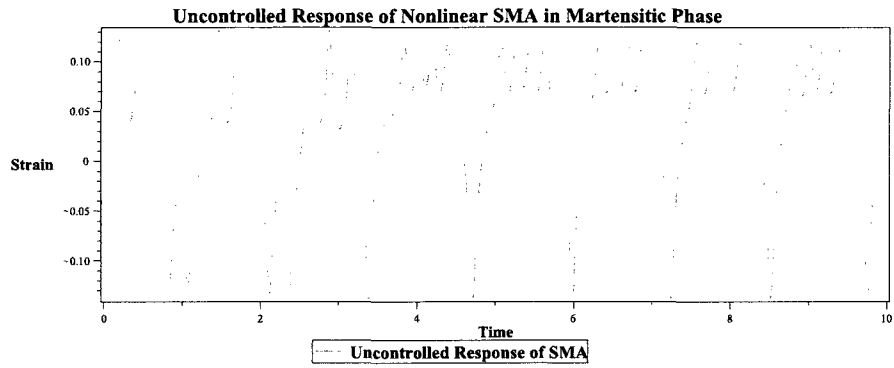


Figure 3.2: Uncontrolled response of the SMA in its martensitic phase

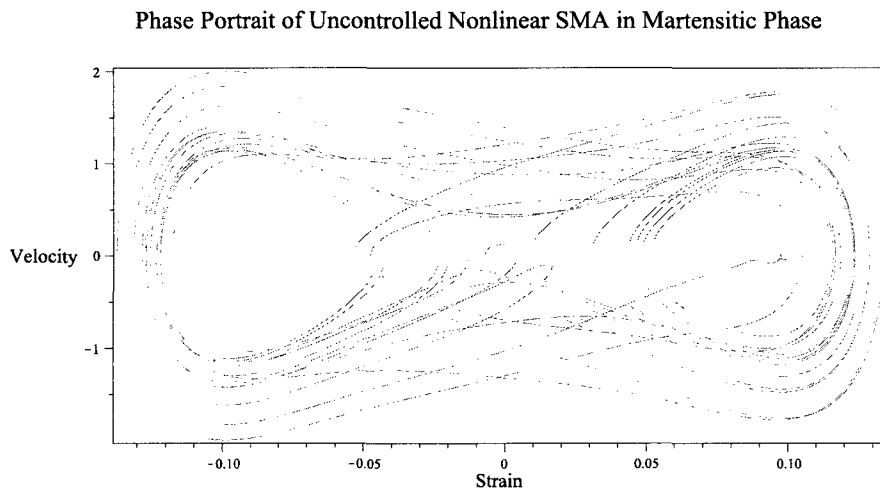


Figure 3.3: Phase portrait of the uncontrolled SMA in its martensitic phase

oscillates in an irregular manner, it evolves over time so that any given region eventually overlaps with any other region. Tests of the model also showed that the response of the SMA is sensitive to changes in the initial conditions. These are some of the properties of chaotic behavior as defined in [51], in fact a number of studies (see e.g [58, 66, 68]) confirmed the presence of chaos in SMA systems. The chaotic behavior of the dynamical system represented by the model (3.2) can also be determined in terms of the Lyapunov exponents, which provide a qualitatively picture of the system's dynamics [36, 58]. We will assume that the response of the SMA system is chaotic without resorting to the Lyapunov exponents method, and for further details about the method and the algorithm for the estimation of the Lyapunov exponents one can refer to ([36] pages 174–175). The chaotic response of SMAs prohibits their use in many engineering, biomedical, and scientific applications, despite their unique properties. In order to utilize these unique properties, especially the SME in our case, which gives rise to the actuation needed to pull mass m of the 1 DOF oscillator, one needs to find ways to eliminate the chaotic behavior. In Chapter 4, we will use linear optimal control methods to design a LQR controller that eliminates the chaotic behavior and tracks the response of the 1 DOF oscillator to a stable equilibrium.

3.3 Analysis of the Austenitic Phase

We will now analyze the response of the SMA system described by equation (3.2) when it exists in the austenitic phase. This can be done by assigning a value to temperature T in the region where the SMA exists in the austenitic phase only. We already know from section 2.3 Chapter 2 that SMAs exist in the austenitic phase at

Table 3.2: Material Constants of Cu-Zn-Al-Ni SMA in Austenitic Phase [57]

| Parameters | Values |
|------------|----------------------|
| a | 1 MPa |
| b | 40×10^3 MPa |
| T_M | 287 K |
| T_A | 364 K |
| T | 400 K |

high temperatures if $T \geq T_A$. The numerical results presented in Figures 3.4 and 3.5 were obtained by choosing the appropriate temperature T , and the numerical values of the SMA parameters, a, b, T_M , T_A given in Table 3.2. Similarly to the study of the SMA in its martensetic phase, the parameters are substituted in the dynamic equation of the system, equation (3.2), and choosing a similar input function $u(t) = 10 \sin(5t)$ we get a second order nonlinear differential equation that represents the SMA in its austenitic phase:

$$\frac{d^2}{dt^2}x(t) + 0.2 \frac{d}{dt}x(t) + 150x(t) - 40000.0x(t)^3 + 5194805.195x(t)^5 = 10 \sin(5t). \quad (3.4)$$

The numerical results representing the response of the SMA in its austenitic phase are shown in Figures 3.4 and 3.5. The response of the SMA in its austenitic phase is also oscillatory and chaotic, a behavior that hinders their use in many engineering and scientific applications. The difference between the responses of the SMA in the martensetic and the austenitic phases, is that in the martensetic phase the SMA's response evolves around two stable states representing the two variants of the martensite phase, while in the austenitic phase the response of the SMA evolves around a

Uncontrolled Response of Nonlinear SMA in Austenetic Phase

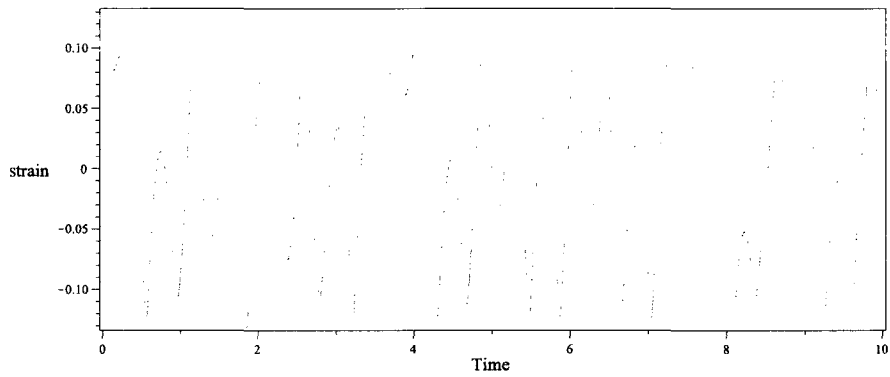


Figure 3.4: Uncontrolled response of the SMA in its austenetic phase

single stable state. These results confirm the discussion of the polynomial constitutive model presented in section 1.2.1 of Chapter 1.

Phase Portrait of Uncontrolled Nonlinear SMA in Austenetic Phase

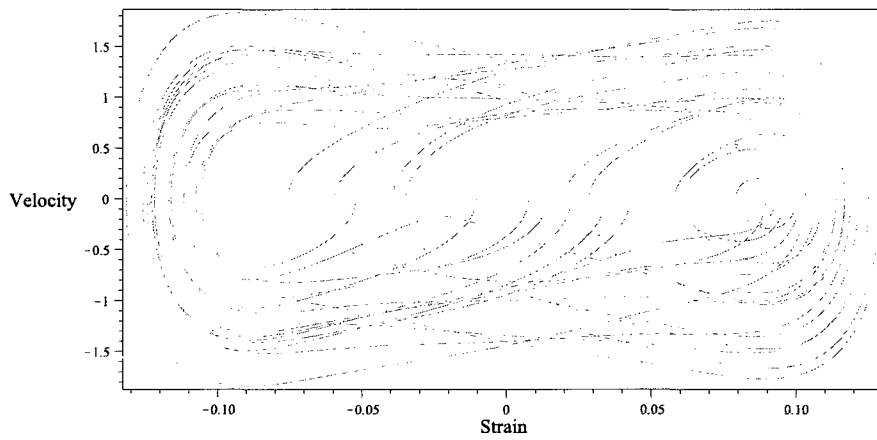


Figure 3.5: Portrait of the uncontrolled SMA in its austenetic phase

Based on the analysis of the SMA's response in its two phases, martensite and

austenite, it is clear from the response of the system that the behavior of the SMA is oscillatory and unpredictable. Therefore, to benefit from the unique properties of SMAs, such as the shape memory effect and pseudo-elasticity, we need to develop a controller to stabilize the system and eliminate the chaotic behavior.

3.4 Summary

In this chapter we have focused on the dynamic response of a 1 DOF oscillator where the nonlinear restoring force is provided by a spring with shape memory. The behavior of the spring with shape memory is described through the Falk polynomial constitutive model. The system is then mathematically described by a second order nonlinear differential equation which was then solved using Maple's numeric differential equation solver *RKF45*. From the numerical results presented in Figures (3.2)–(3.5), we concluded that the response of the system is chaotic and unpredictable. In the next chapter we will focus on the design and implementation of a linear optimal controller with the aim to eliminate or compensate for the chaotic behavior.

Chapter 4

Optimal Control

In Chapter 3 we developed a model for a 1 DOF nonlinear oscillator with a SMA element based on Falk's polynomial constitutive model. The model was analyzed numerically by choosing a temperature where the SMA exists in either its martensitic or austenitic phase. The simulation results presented in Figures (3.2–3.5) showed that, due to the hysteresis phenomenon of SMAs, the response of the system is chaotic and unpredictable. Therefore, the effectiveness of SMAs is hampered, making them difficult to use without some form of control. In this chapter we will address the issue of hysteresis of SMAs from a control perspective.

While design, modeling and dynamics of SMAs have been studied extensively, there is still a great deal of open questions, in particular in the area of control of SMA dynamics. Analysis and control design of nonlinear systems are among the most challenging problems in systems and control theory [59, 60]. For SMAs in particular, control design is a very difficult problem to solve for three main reasons [12, 40]:

- SMAs present complex thermo-electro-mechanical dynamics that are difficult

to model;

- Due to their temperature dependency, SMAs are very sensitive to temperature changes;
- Due to the flexible characteristics of SMAs, substantial vibrations can be excited when the SMA is used as an actuator;
- Controllers for SMA devices need to be robust in system and environmental changes and modeling errors.

In the past there has been a number of studies into control of systems with shape memory alloys in particular in [12, 30, 57, 74]. In [57] (see also references therein) for instance, the authors discussed a number of different strategies that were applied to systems with SMAs. These include the application of a proportional derivative (PD) control scheme to SMA wires used as actuators of a biped walking robot. An active proportional integral derivative (PID) control was used on a segmented active endoscope made with SMA springs, a proportional integral (PI) control was used on SMA actuators with an additional thermal sensor, and a very simple proportional (P) control was used to verify the SMA system model and analyze the system's stability. The control gains are tuned through simulations with trial and error method. The drawback of linear P, PI or PID control is that the controller may perform well in the range where the control gains are tuned, but deteriorates dramatically once outside that range [40].

Also, various adaptive control algorithms have been proposed for use in the application of SMAs. In [12] for example, an adaptive control was used to compensate

directly the hysteresis of SMAs when these actuators are used in vibration suppression applications. In [30] (see also references therein), the authors took into account in their adaptive control algorithm the estimation of thermal changes between the SMA actuators and the environment and calculated the compensating input using an established SMA model. The drawback of this method is that the model and the calculations are very complicated, thus increasing the burden for computation in experimental implementations [40, 74].

In [74] (see also references therein) the authors used feedback linearization of the state equations by introducing a feedback which is a nonlinear function of the system states. The nonlinear factors introduced by the feedback aim at compensating the original nonlinear factor. Due to the hysteretic nature of SMAs, we have seen in the pervious chapter that the response of the nonlinear oscillator defined by equation (3.2) is chaotic and unpredictable (see Figures 3.2–3.5). In order to make use of the SMA in an effective way we need to deal with the hysteresis phenomenon that is the main cause of the nonlinearity in this case. To achieve this objective, a controller will be designed and implemented to move the system defined by equation (3.2) from the chaotic unstable state to a desirable stable state. Generally speaking, there are two ways to deal with hysteretic nonlinearities [12, 80]:

- Open-loop compensation: Find a first-principle or phenomenological model, if possible, to remove or at least ameliorate the nonlinearity.
- Closed-loop feedback: Use the output error (measured output subtracting the desired output) to generate the corrective input.

We will consider the closed-loop feedback method to deal with the nonlinearity of the nonlinear SMA oscillator discussed in the Chapter 3. In the coming sections, an optimal linear quadratic regulator (LQR) controller will be designed and applied to the system given by equation (3.2). The mathematical model of the closed-loop system will be derived and simulated, and the results will be presented.

4.1 Linear Quadratic Regulator Control Design

In an optimal control problem one attempts to find a controller which causes a given system to follow a trajectory that provides the best possible performance with respect to some given measure of performance [26].

The LQR optimal feedback is one of many methods to improve stability performance of any unstable system. Using LQR theory, it has been established that for a controllable linear time-invariant system, a set of optimal feedback gains may be found which minimize a quadratic index and makes a closed system stable by way of Lyapunov function as described in section 2.2 of Chapter 2 [4, 34].

We opted for an LQR controller design because it is easy to design and implement, and in our case it will improve the stability performance by compensating for the hysteretic relationship between input and output of the SMA system. The controller will perform as long as the system is controllable¹ and observable [23]. We will next cover all the steps involved in designing an LQR controller, which we will then apply to the nonlinear oscillator system described by equation (3.2) with the objective to find a control law that moves the system from the uncontrolled chaotic state to a

¹Controllability and Observability will be discussed in section 4.3

stable one, in this case a stable equilibrium.

Since the system described by (3.2) is nonlinear, the first step to designing an LQR controller is to linearize the system. Applying the linearization steps, which will be discussed in section 4.2, to the nonlinear system described by equation (3.2) gives a system of first order differential equations in the form:

$$\dot{\vec{x}}(t) = A \times \vec{x}(t) + B \times \vec{u}(t), \quad (4.1)$$

where $\vec{x}(t)$ is the state vector, $\vec{u}(t)$ is the control vector, and A and B are two real matrices, that may be constants or time dependent, and whose dimension is consistent with the dimension of the state and input vectors.

For an LQR controller the objective is to minimize a particular performance measure. In our case the performance measure will be to minimize the energy of the controlled output \vec{x} and the energy of the control signal \vec{u} of the SMA system. Therefore, the performance measure is given by the standard expression [4, 24, 57]:

$$I = \int_0^{\infty} (\vec{x}(t))^T Q \vec{x}(t) + (\vec{u}(t))^T R \vec{u}(t) dt, \quad (4.2)$$

subject to (4.1) and the initial condition $\vec{x}(0) = \vec{x}_0$, where Q is a real symmetric positive semi-definite weighting matrix and R is a real symmetric positive definite weighting matrix, and \vec{x}_0 is the initial state of the system. The control law for the LQR controller is a linear time-varying function of the system states, see ([26], pages 209 – 227), and is given by:

$$\vec{u}^*(t) = -K \vec{x}(t), \quad (4.3)$$

where K is the gain matrix given by:

$$K = R^{-1} B^T P, \quad (4.4)$$

and P is found by solving the algebraic Riccati equation;

$$A^T P + PA - PBR^{-1}B^T P + Q = 0. \quad (4.5)$$

Before we begin the design and implement the LQR controller into the 1 DOF nonlinear oscillator we need to linearize the system. Linearization of the system will be discussed in section 4.2 and a linear approximation of the nonlinear oscillator will be derived.

4.2 System Linearization

Although almost every physical system contains nonlinearities, oftentimes its behavior within a certain operating range of an equilibrium point can be reasonably approximated by that of a linear model. One reason for approximating a nonlinear system by a linear model is that, by doing so, one can apply rather simple and systematic linear control design techniques, keeping in mind, however, that a linearized model is valid only when the system operates in a sufficiently small range around an equilibrium point. Linearization involves converting a given nonlinear differential equation into a system of first order differential equations, known as state-space form. The resulting system of equations is then solved to find the equilibrium points. Finally, a stable equilibrium is chosen and the system is linearized about this equilibrium to obtain a linear approximation of the nonlinear system. The dynamic equation of the nonlinear oscillator with the SMA device given in equation (3.2) is in the form:

$$\dot{\vec{x}}(t) = f(\vec{x}(t), \vec{u}(t)), \quad (4.6)$$

where $f(\vec{x}(t), \vec{u}(t))$ is a vector function of the state vector $\vec{x}(t)$ and the control vector $\vec{u}(t)$ given by equation (4.9) .

To linearize the system described by the equation (3.2), we will follow the steps described in sections 4.2.1–4.2.3:

4.2.1 State-Variable Form

The first step in linearizing a nonlinear system is to convert it into a set of first order differential equations. This is achieved by letting:

$$x_1 = x(t), \quad x_2 = \dot{x}(t). \quad (4.7)$$

We then take the first derivative of x_1 and x_2 with respect to time and substitute in equation (3.2), this gives the new system of first order differential equations (4.8):

$$\begin{bmatrix} \dot{x}_1(t) \\ \dot{x}_2(t) \end{bmatrix} = \begin{bmatrix} x_2 \\ -cx_2 - a(T - T_M)x_1 + bx_1^3 - \frac{b^2x_1^5}{4a(T_A - T_M)} \end{bmatrix} + u(t) \begin{bmatrix} 0 \\ 1 \end{bmatrix}. \quad (4.8)$$

Therefore, the vector function f is given by:

$$\begin{bmatrix} f_0(x_1, x_2) \\ f_1(x_1, x_2) \end{bmatrix} = \begin{bmatrix} x_2 \\ -cx_2 - a(T - T_M)x_1 + bx_1^3 - \frac{b^2x_1^5}{4a(T_A - T_M)} \end{bmatrix}, \quad (4.9)$$

where a , b , T_M , and T_A are parameters of the SMA, and T is the temperature parameter.

4.2.2 Finding Equilibria

The next step is to find the equilibria of the system by solving the system of equations (4.9) for x_1 and x_2 :

$$\begin{cases} f_0(x_1, x_2) = 0, \\ f_1(x_1, x_2) = 0. \end{cases} \quad (4.10)$$

4.2.3 Stability Check

If x^* is an equilibrium of the the system of equations (4.10), its stability is determined by computing the Jacobian J of the system at this equilibrium, where the Jacobian is given by the following standard expression:

$$J = \begin{bmatrix} \frac{\partial}{\partial x_1} f_0(x_1, x_2) & \frac{\partial}{\partial x_2} f_0(x_1, x_2) \\ \frac{\partial}{\partial x_1} f_1(x_1, x_2) & \frac{\partial}{\partial x_2} f_1(x_1, x_2) \end{bmatrix}. \quad (4.11)$$

Next we recall the following result:

Theorem 2 [26]: *An equilibrium is stable if and only if the real part of the eigenvalues of its corresponding Jacobian matrix are all negative.*

The nonlinear system described by equation (3.2) can now be approximated by a linear system in the form of equation (4.1), where $\vec{x}(t)$ is the state vector of the system, the matrix A is obtained by computing the Jacobian J at the stable equilibrium, and B is the vector of input controls.

Note that since we are dealing with a system with two phases, martensite and austenite, we will compute the matrix A for each phase.

Before we proceed to the design of the LQR controller for our system we need to check

first if the system is controllable and observable. The controllability and observability of the system will be discussed in section 4.3.

4.3 Controllability and Observability

In many control engineering applications, the task of a control engineer is to design a controller to interact with the pre-existing system. However, some systems simply cannot be controlled. The concept of controllability refers to the ability of a controller to move the system from an initial state to another state over a finite time [33]. In other words if we assume that the system is at the origin initially, can we find a control signal so that the state reaches a given position at a fixed time. We follow [9, 26, 33] to define controllability and observability of a dynamic system.

Definition 3 [26]: *A linear system in the form of equation (4.1) is controllable if for any $[x_0, x_f] \in \mathbb{R}^n$ and any time $T > 0$ there exists an input $u : [0, T] \rightarrow \mathbb{R}$ such that the solution of the dynamics starting at the initial condition $x(0) = x_0$ and applying input $u(t)$ gives $x(T) = x_f$. The controllability of the dynamical system is defined in terms of states and does not depend on the output.*

Theorem 3 [26]: *A linear system is controllable if and only if the rank of the $n * n$ controllability matrix:*

$$C = \begin{bmatrix} B & A \times B & A^2 \times B & \dots & A^{n-1} \times B \end{bmatrix} \quad (4.12)$$

is equal to n .

Definition 4 [26]: *Observability of a linear system in control theory is a measure for how well internal states of a system can be inferred by knowledge of its external outputs. The observability and controllability of a system are mathematical duals.*

Theorem 4 [26]: *A linear system in the form of equation (4.1) is observable if and only if the rank of the observability matrix:*

$$O = \begin{bmatrix} C \\ C \times A \\ C \times A^2 \\ \vdots \\ C \times A^{n-1} \end{bmatrix} \quad (4.13)$$

is equal to n .

Now that we defined the steps needed to design an LQR controller, in section 4.4 we will implement these steps to design a controller for the nonlinear oscillator with the SMA element while it exists in one of its two phases, martensite or austenite.

4.4 LQR Design of the Martensite Phase

The phase of the SMA is determined by the change in temperature, for high temperatures the SMA exists in its austenitic phase, and at low temperatures it exists in its martensitic phase. To simulate the response of the SMA in the martensitic phase we assume that the temperature T is constant and is set to a value where the SMA exists in its martensitic phase. The martensitic phase is stable when $T < T_M$, where T_M is the temperature below which the martensitic phase is stable. The SMA

used in our analysis has $T_M = 287K$ (see Table 3.1), so by choosing a temperature $T = 283K$ the SMA is in its martensitic phase. In this section we will implement the steps defined in sections 4.2 and 4.3 to design an LQR controller for the martensitic phase of the SMA. We will begin by finding a linear approximation of the SMA in its martensitic phase, then check whether the approximated system is controllable and observable. We then compute the controller gain K using equation (4.18) and simulate the closed-loop response of the system. The numerical results are obtained using the following Maple routines: for controllability and observability the Maple routines “ControllabilityMatrix” and “ObservabilityMatrix” are used, and for the controller gain K the Maple routine “LQRController” is used. The Maple codes for all the routines developed in this context are included in Appendix B.

Applying the linearization steps discussed in section 4.2 to the martensitic phase model given by equation (3.3), we get the following linear approximation at the equilibrium point ($x_1 = 0.0525, x_2 = 0$):

$$\begin{bmatrix} \dot{x}_1(t) \\ \dot{x}_2(t) \end{bmatrix} = \begin{bmatrix} 0 & 1 \\ -237.0539232 & -0.2 \end{bmatrix} \begin{bmatrix} x_1 \\ x_2 \end{bmatrix} + u(t) \begin{bmatrix} 0 \\ 1 \end{bmatrix}. \quad (4.14)$$

Therefore, the matrices A and B of the approximated linear system are:

$$A = \begin{bmatrix} 0 & 1 \\ -237.0539 & -0.2 \end{bmatrix}, \quad B = \begin{bmatrix} 0 \\ 1 \end{bmatrix}. \quad (4.15)$$

Now based on (4.12) and (4.13), the system’s controllability matrix C and the observability matrix O are:

$$C = \begin{bmatrix} 0 & 1 \\ 1 & -0.2 \end{bmatrix}, \quad O = \begin{bmatrix} 1 & 0 \\ 0 & 1 \end{bmatrix}. \quad (4.16)$$

The rank of matrix C and O is 2, therefore the system is controllable and observable. The optimal control law that minimizes the performance measure I given in equation (4.2) is a linear time-varying function of the system states [26] and is given by:

$$\vec{u}^*(t) = -K\vec{x}(t), \quad (4.17)$$

where K is the gain matrix given by:

$$K = R^{-1}B^T P, \quad (4.18)$$

and P is found by solving the continuous time algebraic Riccati equation

$$A^T P + PA - PBR^{-1}B^T P + Q = 0. \quad (4.19)$$

The matrix Q in equation (4.19) quantifies the divergence of system state, whereas R specifies the cost of the control effort. A suitable choice of Q and R leads to the computation of the controller gain K . If the components of Q are chosen large relative to those of R , then deviations of x will be penalized heavily relative to deviations of u . On the other hand, if the components of R are large relative to those of Q , then control effort will be more costly. Q and R are usually chosen randomly [39, 49, 57], keeping in mind that Q is chosen as a real symmetric positive semi-definite matrix and R is a scalar real value. In our simulation the Q and R matrices used in LQR design are selected as follows:

$$Q = \begin{bmatrix} 10 & 0 \\ 0 & 10 \end{bmatrix}, \quad R = 0.1. \quad (4.20)$$

Using the Maple routine "LQRController" the gain matrix K is computed to be:

$$K = \begin{bmatrix} 0.0422 & 4.2860 \end{bmatrix}. \quad (4.21)$$

Therefore, the control law is given by:

$$\bar{u}^*(t) = -0.0422 x_1(t) - 4.2860 x_2(t). \quad (4.22)$$

4.5 Closed-loop Feedback Response of the Martensitic Phase

Now that we found the control law that optimizes the linearized system, the closed-loop representation of our system is found by substituting the input variable $u(t)$ by the new control variable $\bar{u}^*(t)$ given by equation (4.22) in the equation representing the martensitic phase. The resulting controlled system is:

$$\left[\begin{array}{l} \frac{d}{dt} x_1(t) = x_2(t) \\ \frac{d}{dt} x_2(t) = 3.957819258 x_1(t) - 4.4860 x_2(t) + 40000.0 (x_1(t))^3 - 15000000.0 (x_1(t))^5 \end{array} \right] \quad (4.23)$$

The response of the controlled system is then given by solving the new system of differential equations (4.23) and the results are shown in Figures 4.1, 4.2. From the phase portrait, shown in Figure 4.2, of the closed-loop system given by equation (4.23) we observe that starting the system at the initial condition $x_0 = 0.01$ the feedback control moved the 1 DOF nonlinear oscillator with SMA from the chaotic unpredictable state to the stable equilibrium ($x_1 = 0.0525, x_2 = 0$). This indicates that if we choose a region of operation around an equilibrium point, the LQR controller does indeed stabilize the system in the vicinity of the equilibrium point. This means that by linearizing the 1 DOF nonlinear oscillator around a stable equilibrium and using an LQR feedback control we managed to change the dynamics of the system.

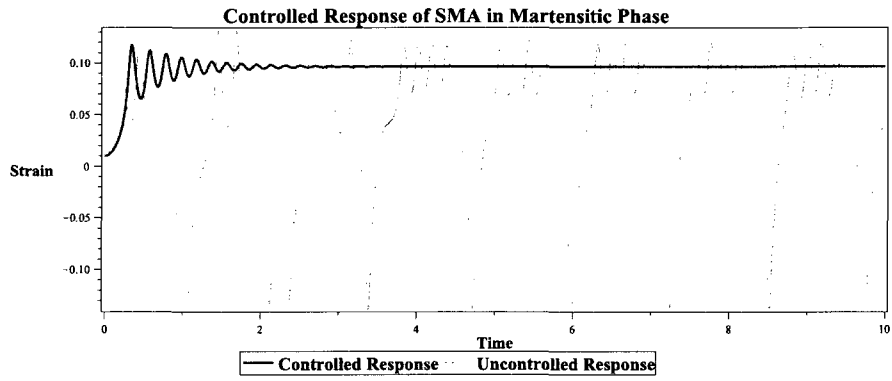


Figure 4.1: Controlled and Uncontrolled Response of the Nonlinear Oscillator “Martensitic Phase”

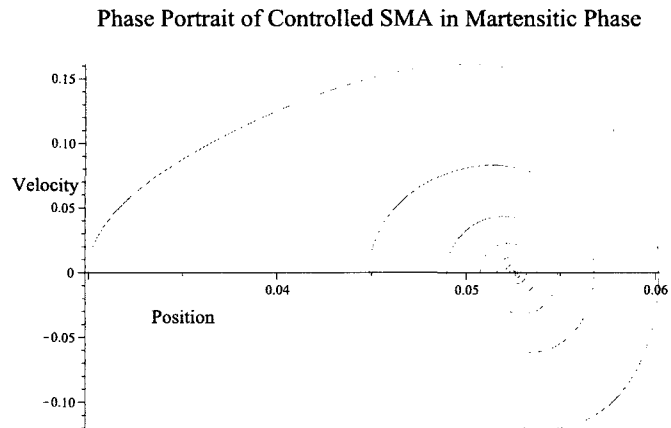


Figure 4.2: Phase Portrait of the Controlled Nonlinear Oscillator “Martensitic Phase”

4.6 Stability by Lyapunov Method

Having formulated the control problem for the martensitic phase in sections 4.4–4.5, and numerical results of the controlled response of the SMA in its martensitic phase were presented in Figures 4.1 and 4.2, we now need to show that the closed-loop response of the controlled system is stable. The most necessary and sufficient condition for stability of dynamic systems is the existence of a Lyapunov function [17, 25, 82]. In Chapter 2 section 2.2, we discussed the stability of dynamic systems by way of Lyapunov method as described by definition (2) and theorem (1). Choosing a Lyapunov function is not always straightforward, however for linear systems the theory is well established [82]. For linear dynamic systems, the Lyapunov function is chosen as a quadratic function in terms of the state vector \vec{x} of the dynamic system and the matrix P which is the solution of the Riccati equation. Following this rule and using the Lyapunov stability definition, we will consider the following Lyapunov function to prove stability of the controlled dynamic system given by (4.23):

$$V(\vec{x}) = \vec{x} P \vec{x}, \quad (4.24)$$

where \vec{x} is the state vector of the dynamic system described by equation (4.14) and P is the solution of the Riccati equation give by (4.19), and is at least positive definite. By solving the the Riccati equation (4.19) for P we get the following matrix:

$$P = \begin{bmatrix} 9.45 & 3.16 \\ 3.16 & 9.45 \end{bmatrix}, \quad (4.25)$$

and substituting P in (4.24) we get:

$$V(x_1, x_2) = 9.45 x_1^2 + 6.32 x_1 x_2 + 9.45 x_2^2. \quad (4.26)$$

Clearly, $V(x)$ is positive definite, and $V(0) = 0$. Differentiating $V(x)$ along the trajectory of the system gives:

$$\dot{V}(x_1, x_2) = -4473.213147 x_1 x_2 - 16.08952081 x_2^2 - 1499.527547 x_1^2. \quad (4.27)$$

$\dot{V}(x)$ is negative, therefore the closed-loop response of the system (4.23) is stable.

4.7 LQR Design of the Austenitic Phase

Since the SMA exists in its austenitic phase when the temperature $T > T_A$, the SMA used in our systems has $T_A = 362.2K$, so by choosing a temperature $T = 400K$ the SMA is in its austenetic phase. We proceed here in a similar way as for the martensitic phase to derive the equations of the linearized model.

System's linearization gives:

$$\begin{bmatrix} \dot{x}_1(t) \\ \dot{x}_2(t) \end{bmatrix} = \begin{bmatrix} 0 & 1 \\ -113 & -0.02 \end{bmatrix} \begin{bmatrix} x_1 \\ x_2 \end{bmatrix} + u(t) \begin{bmatrix} 0 \\ 1 \end{bmatrix}. \quad (4.28)$$

Therefore, the matrices A and B of the approximated linear system are:

$$A = \begin{bmatrix} 0 & 1 \\ -113 & -0.02 \end{bmatrix}, B = \begin{bmatrix} 0 \\ 1 \end{bmatrix}. \quad (4.29)$$

Based on definitions (4.12) and (4.13) the controllability and observability matrices of the 1 DOF nonlinear oscillator, when the SMA is in its astenitic phase, are given by:

$$C = \begin{bmatrix} 0 & 1 \\ 1 & -0.02 \end{bmatrix}, O = \begin{bmatrix} 1 & 0 \\ 0 & 1 \end{bmatrix}. \quad (4.30)$$

The rank of matrix C and O is 2, therefore the system is controllable and observable. The optimal control law that minimizes the performance measure I given in equation (4.2) is a linear time-varying function of the system states [26] and is given by equations (4.17)–(4.19): The matrix Q in the Riccati equation (4.19) is chosen as a diagonal matrix and R is a scalar real values given now as:

$$Q = \begin{bmatrix} 1 & 0 \\ 0 & 1 \end{bmatrix}, R = 1. \quad (4.31)$$

Using the Maple routine "LQRController" the gain matrix K is computed to be:

$$K = \begin{bmatrix} 0.0422 & 4.2860 \end{bmatrix}. \quad (4.32)$$

Therefore, the control law in this case is given by:

$$\bar{u}^*(t) = -0.00422 x_1(t) - 0.985 x_2(t). \quad (4.33)$$

4.8 Closed-loop Feedback Response of the Austenitic Phase

Similar to section 4.5, the closed-loop representation of our system is found by substituting the input variable $\bar{u}(t)$ by the new control variable $\bar{u}^*(t)$ given by equation (4.33) in the equation representing the austenitic phase.

The new system of first order differential equations is given by:

$$\left[\begin{array}{l} \frac{d}{dt} x_1(t) = x_2(t) \\ \frac{d}{dt} x_2(t) = -113.002 x_1(t) - 0.842 x_2(t) + 40000.0 (x_1(t))^3 - 5194805.195 (x_1(t))^5 \end{array} \right], \quad (4.34)$$

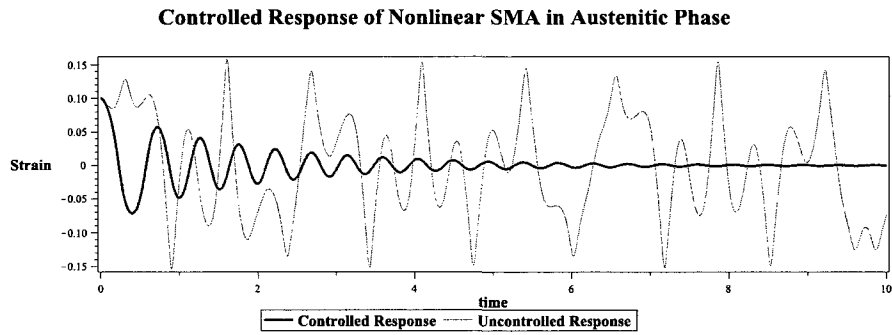


Figure 4.3: Controlled and Uncontrolled Response of the Nonlinear Oscillator “Austenitic Phase”

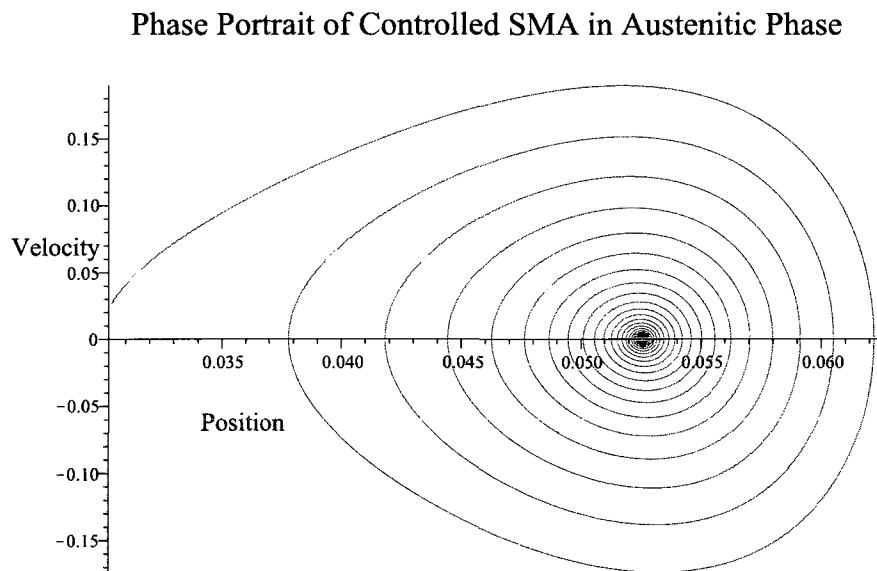


Figure 4.4: Phase Portrait of The Controlled Nonlinear Oscillator “Austenitic Phase”

and the response of the controlled system is shown in Figures 4.3 and 4.4.

As with the SMA in the martensitic phase, when it is in its austenetic phase the response of the uncontrolled system was chaotic and unpredictable. The model was then linearized around the equilibrium point ($x_1 = 0.0525, x_2 = 0$). Using linear feedback control strategy we managed to modify the dynamics of the SMA oscillator. The effect of the LQR controller on the response of the system can be seen in Figure 4.3, which indicates that starting the system from an initial state the system will eventually settle at the stable equilibrium. Stability of the system can be proved by way of a Lyapunov function as in the case of the SMA in the martensetic phase discussed in section 4.6.

4.9 Summary

In Chapter 4 the mathematical model describing a 1 DOF nonlinear oscillator SMA, in either phase, was linearized around the stable equilibrium point ($x_1 = 0.0525, x_2 = 0$). Optimal control was then used to design a LQR controller which was then implemented in a closed-loop feedback control setup to compensate for the hysteretic relationship between input and output of the SMA system. Using LQR optimal control, the unpredictable response of the original system can be controlled to a stable equilibrium as shown in Figures 4.1–4.4. The results show that by using linear feedback control we were able to modify the dynamics of the nonlinear SMA oscillator, and that the proposed method of using a linear quadratic regulator controller was effective in moving the system from the unstable, unpredictable state to a stable controllable state. Based on the results obtained in this chapter we can safely conclude that using

the LQR controller, the SMA can be used as an actuator in a 1 DOF oscillator and its response can be controlled.

Chapter 5

Thermo-mechanical Modeling of SMAs and Model Reductions

In Chapters 3 and 4 a nonlinear oscillator system with a SMA element was modeled, analyzed, and controlled while the SMA was in one of its two phases, martensite or austenite. This was achieved by choosing a temperature where the SMA existed in only one of the phases. In this chapter we will study the thermo-mechanical behavior of the SMA element of the nonlinear oscillator shown in Figure 3.1. As a development of the results obtained in Chapter 3 where the temperature of the SMA was maintained constant, in this chapter the temperature of the SMA will vary by applying a voltage input across it, resulting in the SMA behaving as a transducer converting thermal energy into mechanical energy. In section 5.1, the laws of physics are applied to develop a 1D mathematical model of the SMA as a coupled thermo-mechanical system consisting of a system of PDEs. In section 5.2 the model reduction via Galerkin projection method will be used to transform the system of PDEs into a

set of ODEs that describe the dynamics of the SMA and the heat transfer. In section 5.4 we will also consider an alternative model consisting of three main equations that describe the dynamic characteristics of the SMA [24]. The temperature dynamics are described by Joules heating and natural convection, the mole fraction distribution is given by the Fermi–Dirac statistics that describe a system in two states, and a constitutive equation relating the changes in temperature and mole fraction to the stress and strain induced in the SMA. This model will be used to explain the hysteresis in the SMA as well as the phase transformation and heat transfer.

5.1 Mathematical Model of SMAs

It is well understood that in order to describe the dynamics of SMAs it is important to account for the coupling of the three main physical quantities of continuum mechanics (stresses, deformation gradients, and displacements) to the thermal field [43, 62, 78]. Therefore, to model the dynamics of the SMA sample at the macroscale level accounting for phase transformations, we start from conservation laws for mass and momentum, which will give us the governing equations for the mechanical field. Due to the coupling of mechanical and thermal fields during phase transformations, the governing equation for temperature evolution of the SMA sample should also be added. This can be done using heat equation that is derived by applying the conservation of energy, the first law of thermodynamics and Fourier’s law [13, 24, 32].

5.1.1 Stress–Strain Relation

In order to characterize both, austenite at high temperature and martensite at low temperature, by using a generic expression, the potential energy is constructed on the basis of the modified Landau–Ginzburg free energy function, which reduces to the Falk’s polynomial model discussed in section 1.2.1 of Chapter 1 in the 1D case.

The 1D reduced model can be written as follows [77, 79]:

$$\rho \frac{\partial^2 u}{\partial t^2} = \frac{\partial}{\partial x} \left(k_1 (T - T_M) \left(\frac{\partial u}{\partial x} \right) - k_2 \left(\frac{\partial u}{\partial x} \right)^3 + k_3 \left(\frac{\partial u}{\partial x} \right)^5 \right) + F, \quad (5.1)$$

where ρ is the density of the material, x is the displacement in the x direction, F is the mechanical loading, k_1 , k_2 , and k_3 are material specific parameters and T_M is a reference temperature for the martensite transition.

5.1.2 Heat Conduction

For the heat conduction, we consider the temperature of the SMA to be independent of the strain and martensite–austenite fraction, and to be only a function of the heat transfer. The general solid heat conduction equation is derived by applying the conservation of mass, the first law of thermodynamics and Fourier’s law [32]. Using the electrical charge as the input power, in the 1D case the equation is written as:

$$\rho C_v \frac{\partial T}{\partial t} = k \frac{\partial^2 T}{\partial x^2} - h (T - T_a) + \frac{V^2}{R}, \quad (5.2)$$

where ρ is the material density, T is temperature, C_v is the specific heat coefficient, h is the heat transfer coefficient, T_a is the ambient temperature, and V is the voltage input.

We assume that the transient temperature response of the wire heat conduction in

the direction x can be considered to be much faster than the heat convection (see [32] and reference therein). Therefore, equation (5.2) can be simplified into the following form:

$$\rho C_v V_{SMA} \frac{d}{dt} T(t) = \frac{V^2}{R} - h A_{SMA} (T(t) - T_a), \quad (5.3)$$

where V_{SMA} and A_{SMA} are the total volume and surface area of the SMA. Therefore, the system that describes the coupled thermo-mechanical behavior of the 1D SMA structure can be written as follows:

$$\begin{aligned} \rho \frac{\partial^2 u}{\partial t^2} &= \frac{\partial}{\partial x} \left(k_1 (T - T_M) \left(\frac{\partial u}{\partial x} \right) - k_2 \left(\frac{\partial u}{\partial x} \right)^3 + k_3 \left(\frac{\partial u}{\partial x} \right)^5 \right) + F, \\ \rho C_v V_{SMA} \frac{d}{dt} T(t) &= \frac{V^2}{R} - h A_{SMA} (T(t) - T_a). \end{aligned} \quad (5.4)$$

The numerical results reported in this chapter were performed for a Au-Cu-Zn rod with a length of $L = 1\text{cm}$ and all parameter values are found in [77], in particular the material specific parameters shown in Table 5.1 in section 5.3.

The system of equations (5.4) describing the thermo-mechanical behavior of the SMA system consists of a PDE and an ODE. In the next section we will propose a framework to solve a closed-loop optimal tracking control problem for the system given by equations (5.4). The approach is based on model reduction via the Galerkin projection method to transform the PDE in the system (5.4) into an ordinary differential equation.

5.2 Model Simplification via Galerkin Model Reduction

In this section, we focus on the 1D model given by the system of equations (5.4) over $\Omega = \{(x, t) : 0 \leq x \leq 1, 0 \leq t \leq T\}$.

The system given by equations (5.4) is nonlinear and cannot be solved analytically while its numerical simulation could be a very expensive endeavor. Numerical procedures to find a solution to 1D models describing SMA behavior can be found in articles by a number of authors, in particular in [5, 43, 75–77]. Because of the nonlinear nature of the SMA due to the hysteresis phenomenon, the response of the SMA will have to be controlled in order to make use of the SMA in many applications of these materials. The standard approaches to the control of a system described by a PDE or a system of PDEs involves the application of the standard Galerkin’s projection method to derive a system of ordinary differential equations that accurately describe the dynamics of the system. The resulting system of ODEs is subsequently used as the basis for controller synthesis [3, 64]. Other model reduction methods were discussed where the center manifold reduction was applied to derive a new system of equation. More recently, the Proper Orthogonal Decomposition (POD) [11, 52, 78] for the model reduction of such systems. In section 5.2.3, we will apply the Galerkin reduction method to the model given by equations (5.4) in order to obtain a system of ODEs that will be used as basis for the design of a linear controller for nonlinear systems in Chapter 6.

5.2.1 Galerkin Projection

Before we begin the discussion about the Galerkin Projection method, we briefly highlight the necessary mathematical preliminaries (e.g. [10]):

Definition 5 (Hilbert Space): An Euclidean space \mathbb{R}^n is a vector space endowed with the inner product $\langle x, y \rangle = x^T y$, norm $\|x\| = \sqrt{x^T x} = \sqrt{\langle x, x \rangle}$ and associated metric $\|x - y\|$, such that every Cauchy sequence takes a limit in \mathbb{R}^n . This makes \mathbb{R}^n a Hilbert space. A Hilbert space H is therefore a vector space endowed with an inner product and associated norm and metric, such that every Cauchy sequence in H has a limit in H .

Definition 6 (Inner Product): The inner product serves several purposes in Galerkin procedure. Fundamentally, it helps define the Hilbert space on which the analysis proceeds. It also defines the projection of the governing equations onto the basis, which leads to the Galerkin dynamical model. An inner product on a real vector space V is a real function $\langle x, y \rangle: V \times V \rightarrow \mathbb{R}$ such that for all x, y, z in V and all c in \mathbb{R} ,

- $\langle x, y \rangle = \langle y, x \rangle$
- $\langle cx, y \rangle = c \langle x, y \rangle$
- $\langle x + y, z \rangle = \langle x, z \rangle + \langle y, z \rangle$
- $\langle x, x \rangle > 0, x \neq 0$

For example, in the space $C[0, 1]$ of continuous real functions on $[0, 1]$, the inner product is defined as $\langle f, g \rangle = \int_0^1 f(t) g(t) dt$.

Definition 7 (Orthonormal Basis): Let $V = \{\phi_1, \phi_2, \dots, \phi_n\}$ be a set of continuous functions. The functions ϕ_i of the basis V are said to be orthonormal to each other iff:

$$\langle \phi_i, \phi_j \rangle = \delta_{i,j}, \quad (5.5)$$

where $\delta_{i,j}$ is the Kronecker delta function defined as follows:

$$\delta_{i,j} = \begin{cases} 0 & \text{if } i \neq j \\ 1 & \text{if } i = j \end{cases}.$$

5.2.2 Galerkin Method

Let's now consider a dynamical system which evolves in a Hilbert space H . In particular, for $U(x, t) \in H$, $U(x, t)$ satisfies

$$\begin{aligned} \frac{d}{dt}U(x, t) &= X(U(x, t)), \\ U(t, \partial\Omega) &= 0, \end{aligned} \quad (5.6)$$

where X is a vector field on H . For instance following [3, 52], we note that for a partial differential equation governing variable $U(x, t)$, defined on some spatial domain $x \in \Omega$, H will be a space of functions defined on Ω , and X will be a spatial differential operator. Given a finite-dimensional subspace S of H , Galerkin projection specifies a dynamical system which evolves on S and approximates (5.6) in some sense. This approximate dynamical system is obtained by orthogonal projection of the vector field X onto the subspace. The Galerkin method consists of finding an approximate function $U(x, t)$ over some domain of interest as a finite sum in the variables-separated

form satisfying the boundary conditions of the model given by equation (5.6):

$$U(x, t) \approx \sum_{k=1}^n a_k(t) \phi_k(x), \quad (5.7)$$

where $\phi_k(x)$ are continuous orthonormal functions that form the basis, with the reasonable expectation that the approximation becomes exact in the limit as n approaches infinity. It is well known that the representation of equation (5.7) is not unique. For example, if the domain of x is a bounded interval X on the real line, then the functions $\phi_k(x)$ can be chosen as a Fourier series, or Legendre polynomials, or Chebyshev polynomials, and so on. For each such choice of a sequence $\phi_k(x)$ that forms a basis for some suitable class of functions $U(x, t)$, the sequence of time-functions $a_k(t)$ is different. That is, for sines and cosines we get one sequence of functions $a_k(t)$, for Legendre polynomials we get another, and so on [8, 27].

We substitute the expression (5.7) in equation (5.6):

$$\sum_{i=1}^n \frac{d}{dt} a_i(t) \phi_i(x) = \sum_{i=1}^n X(a_i(t) \phi_i(x)). \quad (5.8)$$

We then write the weak form of equation (5.8) using the inner product discussed in section 5.2.1 by multiplying both sides by $\phi_k(x)$, for $k = 1, 2, \dots, n$, and integrating over the spatial domain, i.e.,

$$\sum_{i=1}^n \frac{d}{dt} a_i(t) \langle \phi_i(x), \phi_k(x) \rangle = \sum_{i=1}^n X(a_i(t) \langle \phi_i(x), \phi_k(x) \rangle), \quad (5.9)$$

where

$$\langle \phi_i(x), \phi_k(x) \rangle = \int_{\partial\Omega} \phi_i(x) \phi_k(x) dx. \quad (5.10)$$

Since the modes $\phi_i(x)$ are orthonormal to each other, from (5.9) $\frac{d}{dt} a_i(t)$ can be approximated by

$$\frac{d}{dt} a_i(t) = \sum_{k=1}^n X \left(a_i(t) \int_{\partial\Omega} \phi_i(x) \phi_k(x) dx \right). \quad (5.11)$$

If we assume Dirichlet boundary conditions on the interval $[0, 1]$, then the orthonormal basis $\phi_k(x) = \sqrt{2} \sin(k\pi x)$ satisfies the boundary conditions and can be used to solve the system of equation given by (5.4). If we substitute the basis $\phi_i(x)$ in equation (5.11) we obtain a set of n ordinary differential equations.

5.2.3 Reduced Order Model

From the system of equations (5.4), we note that the energy equation is a simple ODE which can be solved independently for the temperature T . Therefore, if we apply the Galerkin method described in section 5.2.1, using a first order reduction, to the first equation (PDE) of the system (5.4) relating stress and strain, then the system of equations will be reduced into a system of two ordinary differential equations. Let $\Phi = \{\phi_1 = \sqrt{2} \sin(\pi x), \phi_2 = \sqrt{2} \sin(2\pi x)\}$ be the set of orthonormal basis that will be used for the model reduction using Galerkin method, where ϕ_i are continuous functions on the interval $[0, 1]$. Using this orthonormal basis, we approximate the variable $u(x, t)$ in the PDE describing the dynamics of the SMA as:

$$u(x, t) \approx \sum_{i=1}^2 x_i(t) \phi_i(x). \quad (5.12)$$

Now substituting the expression given by equation (5.13) in the PDE equation given by (5.4) to obtain:

$$\rho \frac{d^2}{dt^2} x_i(t) \sum_{i=1}^2 \phi_i(x) = \frac{\partial}{\partial x} \left[K_1 x_i(t) (T(t) - T_0) \sum_{i=1}^2 \frac{d}{dx} \phi_i(x) - K_2 x_i(t)^3 \left(\sum_{i=1}^2 \frac{d}{dx} \phi_i(x) \right)^3 + K_3 x_i(t)^5 \left(\sum_{i=1}^2 \frac{d}{dx} \phi_i(x) \right)^5 \right] + F. \quad (5.13)$$

The inner product rule defined in section 5.2.1 is then used to write the weak form of equation (5.13) by multiplying both sides by $\phi_1(x)$ and integrating over the spatial

domain $[0, 1]$ to obtain the following ordinary differential equation:

$$\rho \frac{d^2}{dt^2} x_1(t) = \frac{\partial}{\partial x} \sigma + F, \quad (5.14)$$

where σ is given by equation (5.15), which has the form of the polynomial model discussed in section 1.2.1 of Chapter 1 :

$$\sigma = k_1 (T(t) - T_M) x_1(t) - k_2 x_1(t)^3 + k_3 x_1(t)^5. \quad (5.15)$$

The reduced model can be written as follows:

$$\begin{aligned} \rho \frac{d^2}{dt^2} x(t) &= \frac{\partial}{\partial x} \sigma + F, \\ \rho C_v V_{SMA} \frac{d}{dt} T(t) &= \frac{V^2}{R} - h A_{SMA} (T(t) - T_a), \end{aligned} \quad (5.16)$$

where V is the voltage applied across the SMA wire, k_1 , k_2 , and k_3 are parameters of the SMA and R is the material resistance.

The dynamic characteristics of the SMA are defined by the system of equations (5.16) where $x(t)$ is the displacement, $\sigma(t)$ is the stress in the SMA, V is the voltage across the SMA wire, and F is the input load. The SMA model of equations (5.16) is similar to the model given by equation (3.2) that was studied in Chapter 3. The difference is that the new model takes into account the change in temperature using the heat equation that consists of Joule heating and natural convection [13]. In the next section the mathematical model given by (5.16) will be solved numerically and results will be presented.

5.3 Computational Results

In this section the system of equations (5.16) obtained in the previous section is solved using an input F , the force of gravity due to mass m of the nonlinear oscillator in

Table 5.1: Material Constants of Au-Cu-Zn SMA [77]

| Parameters | Values |
|------------|-----------------------------|
| k_1 | $480 \frac{g}{ms^2cmK}$ |
| k_2 | $610^6 \frac{g}{ms^2cmK}$ |
| k_3 | $4.510^8 \frac{g}{ms^2cmK}$ |
| T_M | 208 |
| C_v | $3.1274 \frac{g}{ms^2cmK}$ |
| ρ | $11.1 \frac{g}{cm^3}$ |
| h | $150 \frac{J}{m^2KSec}$ |

Figure 3.1, a voltage $V = 10V$, and the initial conditions given by (5.17). The SMA element used in this analysis is Au-Cu-Zn, and the values of the different parameters of the material can be found in Table 5.1.

$$T(0) = 260K, x(0) = 0.03, x'(0) = 0. \quad (5.17)$$

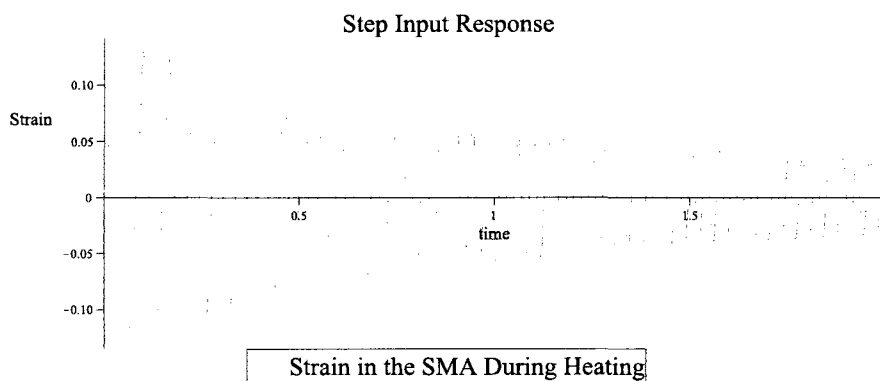


Figure 5.1: Step Response of SMA During Heating of SMA

The results presented in Figure 5.1 show that the response of the SMA system described by the system of equations (5.16) is highly oscillatory. This is mainly due to the dissipative nature of the SMA that results in hysteresis between the input and output of the oscillator. The Figure 5.2 shows the temperature change in the

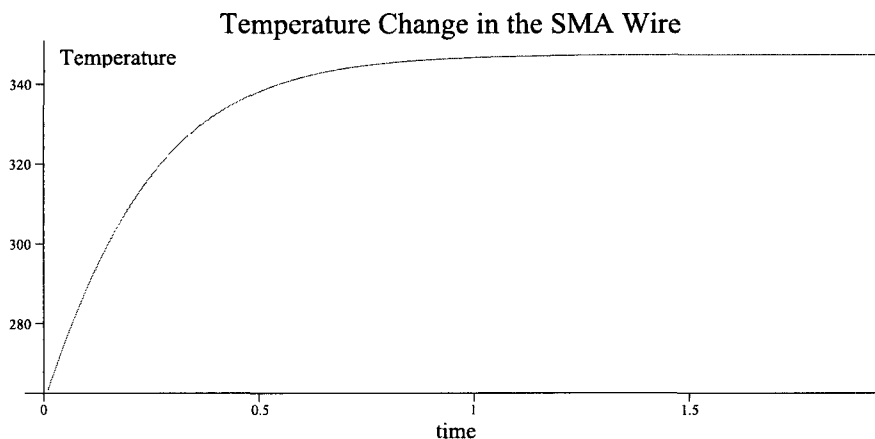


Figure 5.2: Temperature Change During Heating of SMA

SMA element as it is being heated by applying the input voltage V across it. The temperature starts at the initial temperature $T_0 = 260K$ and continues to increase with time causing the SMA to heat up, making the SMA go through a phase transformation.

The Figure 5.3 is the phase portrait representation of the SMA system. From the figure it is clear that the response of the system is chaotic and unpredictable. This shows that despite the excellent properties of the SMAs, their hysteretic nature prohibits them from being used in many applications without adding controllers to compensate for the hysteresis phenomenon.

Phase Portrait of SMA During Heating

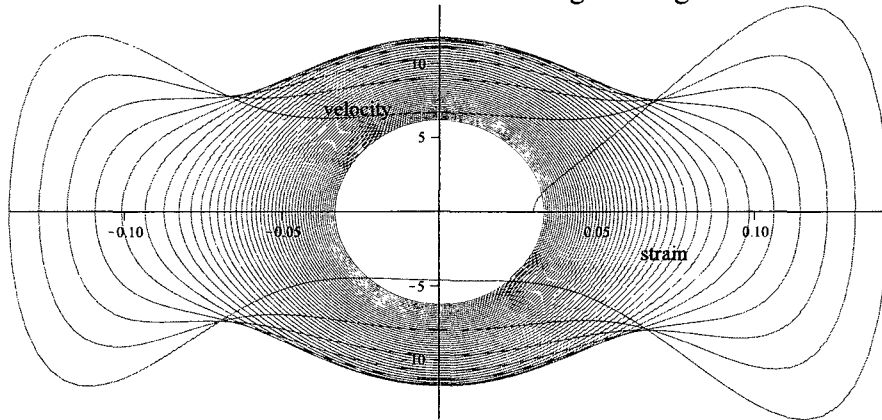


Figure 5.3: Phase Portrait During Heating of SMA

Stress-Strain Curves

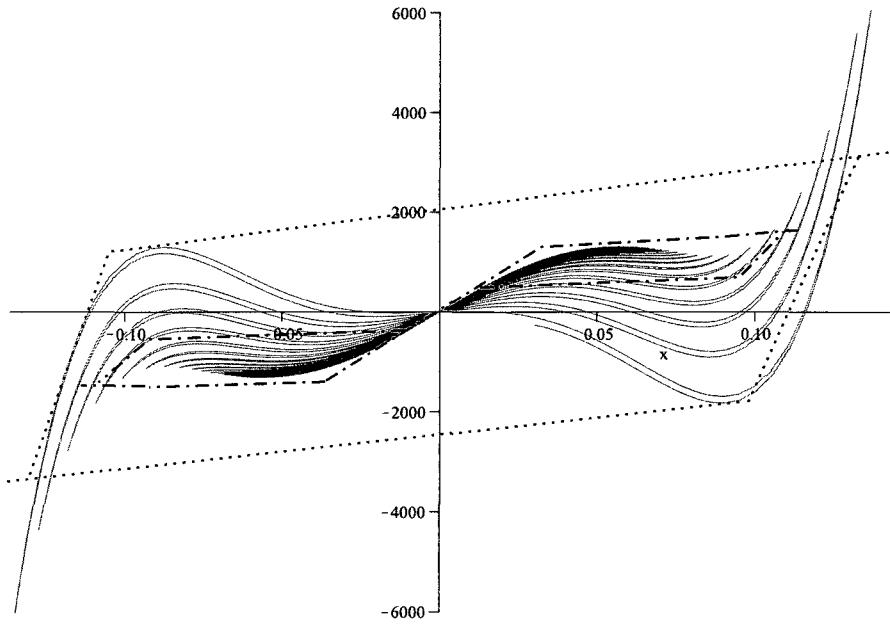


Figure 5.4: Stress-Strain Curves Illustrating SME and Pseudoelasticity

The results presented in Figure 5.4 show the stress-strain relationship of the SMA as it goes from the initial martensitic phase to the austenetic phase. As the temperature increases from the initial temperature $T = 260K$, where the SMA is in its martensitic phase, to $T = 340K$ where the SMA is in its austenitic phase, we see from the figure how the SMA goes through a phase transformation exhibiting shape memory effect as well as pseudoelasticity.

5.4 Thermo-mechanical SMA Model Based on Fermi-Dirac Theory

A new mathematical model of the SMA, based on the Fermi–Dirac model discussed in section 1.2.4 of Chapter 1, will be analyzed in this section. The model consists of three equations, the phase transformation equation described by the Fermi–Dirac model, the Joules heating equation describing the temperature dynamics, and the constitutive equation that relates changes in stress, strain, and phase fraction [24]. The models we examined before were based on the polynomial model discussed in section 1.2.1 where the constitutive model depends on temperature and stress only. The model proposed in this section depends on the stress and temperature, in addition to a variable that represents phase transformation of the SMA. One of the advantages of this model, despite its simplicity, is its ability to capture the properties of the SMA, and it is in the form of a system of ODEs that can be used to design a controller without resorting to model simplification as we have seen in the section 5.2.3.

5.4.1 Phase Transformations

Since a SMA exists only in martensite and austenite phases, it can be modeled as a two-state system, like an electron. The Fermi-Dirac statistics, which describes the distribution of electrons in two states depending on their energy levels, has been found to provide a good model for the state of a SMA in martensite and austenite forms [24]. Since the SMA is in the martensite form at lower temperatures, the phase transformation equation during heating is described by analogy with the Fermi-Dirac statistics in the form;

$$\zeta = \frac{\zeta_m}{1 + e^{\frac{T_{fa}-T}{\sigma_a} + K_a\sigma}}, \quad (5.18)$$

where ζ is the fraction of the austenite phase, ζ_m is the fraction of the martensite phase prior to the present transformation from martensite to austenite, T is the temperature, T_{fa} is the transition temperature from martensite to austenite, σ_a is an indication of the range of temperature around the transition temperature T_{fa} during which the phase change occurs, σ is the stress, and K_a is the stress curve-fitting parameter which is obtained from the stress-strain characteristic with no change in temperature [24]. On cooling, the austenite phase gets converted to the martensitic phase and the modeling equation during cooling is described by analogy with the Fermi-Dirac statistics in the form:

$$\zeta = \frac{\zeta_a}{1 + e^{\frac{T_{fm}-T}{\sigma_m} + K_m\sigma}}, \quad (5.19)$$

where ζ_a is the fraction of the austenite phase prior to the transformation from austenite to martensite, T is the temperature, T_{fm} is the transition temperature from austenite to martensite, σ_m is an indication of the range of temperature around the transition temperature T_{fm} during which the phase change occurs, σ is the stress,

K_m and is the stress curve-fitting parameter which is obtained from the unloading part of the stress-strain characteristic. The parameters K_a and K_b indicate the response of the SMA to application of external stress. Since the SMA is modeled as a two-component system, at any given time the sum of the mole fractions of the austenite and martensite phase is 1, *i.e.*,

$$\zeta_a + \zeta_m = 1. \quad (5.20)$$

The time derivatives of (5.18) and (5.19) are given by equations (1.13) and (1.14) as defined in section 1.2.4 of Chapter 1, where equation (1.13) is used for heating, and equation (1.14) is used for cooling. In equations (1.13) and (1.14) ζ_a is the fraction of the austenite phase prior to the transformation from austenite to martensite, T is the temperature, T_{fm} is the transition temperature from austenite to martensite, σ_m is an indication of the range of temperature around the transition temperature T_{fm} during which the phase change occurs, σ is the stress, K_m is the stress curve-fitting parameter which is obtained from the unloading part of the stress-strain characteristic.

5.4.2 Temperature Dynamics

The SMA actuator is heated by the process of Joules heating by applying a voltage across the SMA. The loss of heat from the SMA is through natural convection. Mathematically the dynamics of the temperature are given by the following equation which has also been used in [13, 24, 30];

$$\frac{d}{dt}T(t) = \frac{1}{m c_p} \left(\frac{V}{R} - (h_0 + h_2 (T(t))^2) (T(t) - T_a) \right), \quad (5.21)$$

where $h = h_0 + h_2 T(t)^2$, h_0 and h_2 are coefficients of convectational cooling of the SMA, V is the voltage across the SMA wire, C_v is the specific heat capacity of the

SMA, and T is temperature.

5.4.3 Constitutive Equation

The constitutive equation relating changes in stress, strain, temperature, and mole fraction is given by equation (5.22) that has been previously used in [24, 53], and was explained in section 1.2.2 of Chapter 1.

$$\frac{d}{dt}\epsilon(t) = \frac{1}{E} \frac{d}{dt}\sigma(t) - \theta_t \frac{d}{dt}T(t) - \Gamma \frac{d}{dt}\zeta(t), \quad (5.22)$$

where σ is the stress in the SMA, D is the Young's modulus of the alloy, ϵ is the strain, θ_t is the thermal expansion factor, $\Gamma = -D\epsilon_i$ is the phase transformation contribution factor, and ϵ_i is the initial strain in the SMA after it had been deformed while in the martensitic phase. The model is capable of explaining the shape memory and super-elastic properties of the SMA. It should be noted here that the modulus of elasticity can be assumed to be the average of the Young's moduli for the martensite and austenite phases to model the shape memory effect while a more precise Young's modulus based on the composition of the alloy would be required to model the super-elastic property. The dynamic characteristics of the SMA can be defined by the system of nonlinear differential equations (1.13), (1.14), and (5.22). The system will then be modeled by considering whether the SMA is being heated or cooled. In the next section numerical results will be presented by solving the system of equations (1.13), (1.14), and (5.22).

5.5 Computational Results

Due to the hysteresis behavior of the SMA wire, two different models will have to be employed for a full cycle simulation, one model representing the SMA as it is being heated and the second one when it is being cooled. Both models will include the constitutive equation (5.22), the heat equation (5.21), and depending on whether the SMA is being cooled or heated we use either equation (1.13) or (1.14). The numerical results presented here are for the SMA when it is being cooled, they are obtained by solving the system of nonlinear differential equations (1.13), (1.14), and (5.22). We notice that as the SMA is being cooled its temperature starts to decrease (see Figure 5.7) resulting in a phase transformation, austenite to martensite (see Figure 5.6). The phase transformation causes a change in the SMA strain as given by the constitutive equation and shown in Figure 5.5. Figure 5.8 shows the relationship between strain and temperature as the SMA is being cooled. The reverse transformation which completes the cycle and shows the strain recovery, not included here, is obtained by solving the model representing the SMA as it is being heated.

The computational results presented in Figures 5.5– 5.8 show that the new model based on the Fermi–Dirac to represent a two-state process provides a good model for the state of a SMA in martensite and austenite forms. We notice that as the temperature, see Fig 5.7, decreases, which corresponds to the cooling process of the SMA, the phase transformation curve 5.6 decreases from 1 towards 0, indicating a phase change from austenite to martensite. Fig 5.8 shows the temperature-strain relationship as the SMA is being cooled, and the reverse process, heating of the SMA while it is in its martensite phase, should complete the hysteresis loop. From the

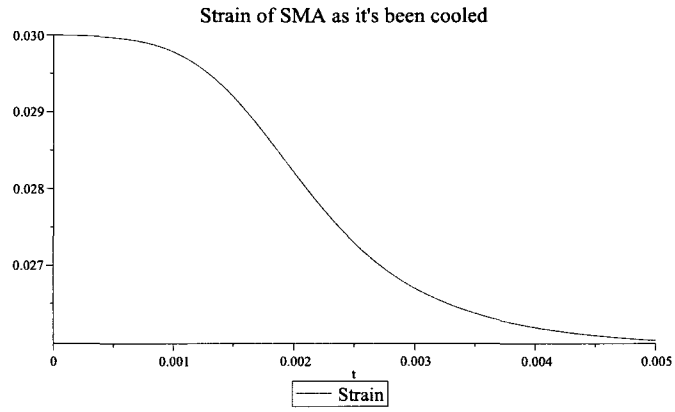


Figure 5.5: Strain of SMA during Cooling

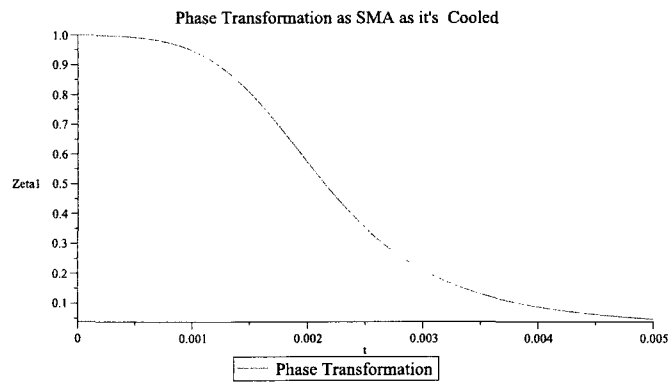


Figure 5.6: Phase transformation of SMA during Cooling

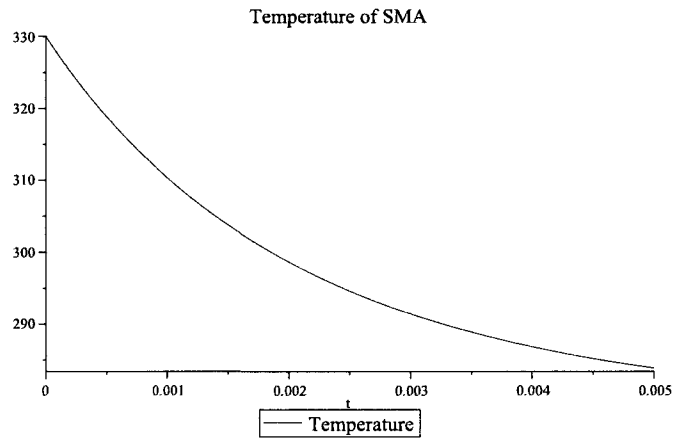


Figure 5.7: Temperature of SMA during Cooling

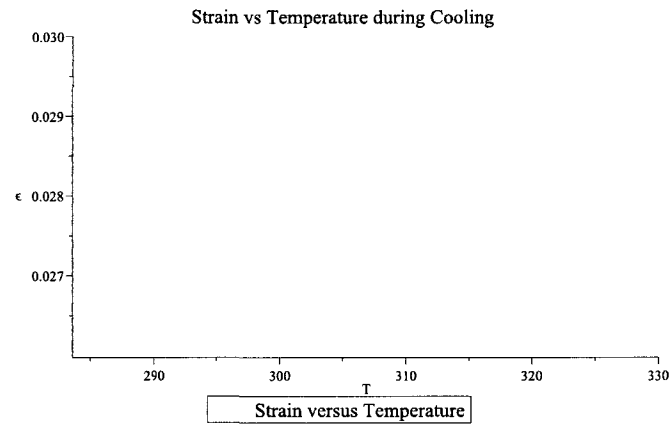


Figure 5.8: Strain versus Temperature of SMA during Cooling

analysis that we have seen so far, SMAs possess some interesting properties that make them suitable candidates for many applications (see Appendix A). However, in many cases, the presence of hysteresis hampers their performance. In order to utilize the SMAs unique characteristics a control strategy must be implemented to eliminate or reduce the inherent hysteresis of SMAs. In the next chapter we will consider the reduced model given by system of ODEs (5.16), and a tracking controller for the system will be designed by using a linear design for nonlinear systems method as described in [39].

5.6 Summary

In Chapter 5 a thermo-mechanical model for the SMA was developed using the conservation laws. The model was then reduced by using the Galerkin method resulting in a system of ODEs, which was then solved and the results were presented in Figures 5.1–5.4. The numerical results presented in section 5.3 were obtained using Maple’s numeric solver “dsolve” that is based on the Runge–Kutta–Fehlberg (*RKF45*) algorithm. Figure 5.1 shows the strain of the SMA as it is been heated, and it is clear that the response is oscillatory and nonstable. Figure 5.2 shows the temperature in the SMA during the heating process. The temperature starts at the initial temperature $T_0 = 260K$ and rises with time until it reaches temperature $T = 340K$. As the temperature changes, we see in Figure 5.4 how the SMA goes through a phase transformation and exhibits shape memory effect and pseudoelasticity. The numerical results show that the response of the uncontrolled SMA is chaotic, which prohibits their use in many applications without resorting to control techniques that would

eliminate or compensate for the nonlinear behavior of SMAs. In Chapter 6 we will develop a feedback control strategy to compensate for hysteretic relation between the input and output of a SMA.

In section 5.4 a different model capable of describing the thermo-mechanical behavior of the SMA was examined. The model is based on the Fermi-Dirac statistics, which describes the distribution of electrons in two states depending on their energy levels. The model was solved numerically and the computational results for heating of the SMA were presented. From Figures 5.6–5.8 we observe that as the temperature started to increase the SMA underwent a phase change. This was noticed as the martensitic phase variable decreased from 1 to almost 0 indicating that the SMA was transformed to the austenitic phase. As the SMA changed phase it recovered its original shape resulting in an actuation that is one of the main applications of SMAs.

Chapter 6

Nonlinear Feedback Control

In Chapter 4 a LQR controller was designed and implemented to stabilize and control a nonlinear 1 DOF oscillator with a SMA. Even though stability of the nonlinear system with SMA was achieved, it is nonetheless local and only valid in the vicinity of the equilibrium point, thus limiting the region of operation of the system. In this chapter we will take a different approach by considering an optimal control strategy of nonlinear systems to design and implement a controller that guarantees global stability of the nonlinear SMA system.

Optimal control of nonlinear systems is one of the most challenging and difficult subjects in control theory. It is well known that the nonlinear optimal control problem can be reduced to the Hamilton-Jacobi-Bellman (HJB) partial differential equation [29, 39, 44, 47, 57, 60], but due to difficulties in its solution, this is rarely a practical approach. Instead, the search for nonlinear control schemes has generally been approached on less ambitious grounds than requiring the exact solution to the HJB partial differential equation [39]. In this chapter, we will consider the system of dif-

ferential equations given by (5.16), with the objective to design a tracking controller to compensate for the hysteresis phenomenon associated with SMAs, and make the SMA system track a given reference input signal. We will use a theorem proposed in [39] that expresses explicitly the form of minimized functional and gives the sufficient conditions that allow using the linear feedback control for nonlinear system. The controlled system will then be simulated and results will be presented in the following sections.

6.1 Linear Design for a Nonlinear System

In Chapter 5 a thermo-mechanical model for the nonlinear oscillator with a SMA was developed using the laws of conservation. The model was then solved numerically and the results were presented in Figures 5.1–5.4. From the numerical results presented in these figures, it is clear that the response is oscillatory and nonstable, and this is mainly due to the hysteretic nature of SMAs. In order to remove or compensate for the hysteretic behavior, an optimal linear control design for nonlinear systems strategy based on the theorem proposed in [39] will be used to design a controller that tracks a reference input signal and guarantees asymptotic stability of the nonlinear SMA system by means of a Lyapunov function.

The thermo-mechanical model developed in Chapter 5 for the nonlinear SMA system given by (5.16) can be written in the following form:

$$\dot{\vec{x}} = A(t)\vec{x} + G(\vec{x}) + B\vec{u}, \quad \vec{x}(0) = \vec{x}_0, \quad (6.1)$$

where \vec{x} is the state vector, $A(t) \in \mathbb{R}^n$ is a bounded matrix and is not unique, whose elements are time dependent, B is a constant matrix, $\vec{u}(t) \in \mathbb{R}^m$ is a control

vector, and $G(\vec{x})$ is a vector, whose elements are continuous nonlinear functions, and $G(0) = 0$. Assume that:

$$G(\vec{x}) = g(\vec{x}) \vec{x}, \quad (6.2)$$

where $g(\vec{x}) \in \mathbb{R}$ is a bounded matrix, whose elements depend on x . Assuming (6.2) we can write the dynamic system (6.1) as follows:

$$\dot{\vec{x}} = A(t) \vec{x} + g(\vec{x}) \vec{x} + B \vec{u}, \quad \vec{x}(0) = \vec{x}_0. \quad (6.3)$$

One of the results that we will use in the subsequent section can be formulated as follows (see proof in [39]):

Theorem 5 [39]

If there exist matrices $Q(t)$ and $R(t)$, positive definite, being Q symmetric, such that the matrix:

$$\tilde{Q} = Q(t) - g(\vec{x})^T P(t) - P(t) g(\vec{x}) \quad (6.4)$$

is positive definite for the bounded matrix g , then the linear feedback control:

$$\vec{u} = R^{-1} B^T P(t) \vec{x} \quad (6.5)$$

is optimal, in order to transfer the non-linear system (6.3) from an initial to final state

$$\vec{x}(t_f) = 0 \quad (6.6)$$

$$J = \int_0^{t_f} \vec{x}^T \tilde{Q} \vec{x} + \vec{u}^T R \vec{u} dt, \quad (6.7)$$

where the symmetric matrix $P(t)$ is evaluated through the solution of the matrix Riccati differential equation:

$$\dot{P}(t) + PA + A^T P - PBR^{-1}P + Q = 0. \quad (6.8)$$

satisfying the final condition:

$$P(t_f) = 0. \quad (6.9)$$

The functional J given by expression (6.7) is in the standard form that was used for the LQR controller in section 4.1 of Chapter 4. The difference between the two functionals is that, in the case of the LQR controller the dynamic equation of the SMA system was linear, whereas the the dynamic equation in this case is nonlinear. The expression of the functional J is made of two terms, the term $\vec{x}^T \tilde{Q} \vec{x}$ corresponds to the energy of the controlled output, and the term $\vec{u}^T R \vec{u}$ corresponds to the energy of the control input. The controller seeks to minimize both energies. However, decreasing the energy of the controlled output will require a large control signal and a small control signal will lead to large controlled outputs. The role of \tilde{Q} and R is to establish a trade-off between these conflicting goals [26, 33]. The controller given by (6.5) minimizes the functional J and guarantees stability by way of Lyapunov function.

In our case we will consider an infinite horizon time by making $t_f = \infty$, and the final state of the system is to track the reference input signal at all times by minimizing the error $\vec{x}(t) - \vec{\tilde{x}}(t)$, where \vec{x} is the state vector and $\vec{\tilde{x}}$ is the reference input signal.

6.2 Linear Design of Nonlinear SMAs

In Chapter 4 we implemented a linear optimal control strategy by designing a LQR controller to stabilize and control the nonlinear 1 DOF oscillator with a SMA. Even though stability of the nonlinear system with SMA was achieved, it is however local and the region of operation of the system is limited. In this section, we will address this issue by considering an optimal linear design control strategy for the nonlinear

system given by equation (5.16). We will apply the proposed linear design for nonlinear systems method stated in section 6.1 to control the nonlinear SMA oscillator, taking into account the change in temperature and how it affects the behavior of the SMA, with the objective to stabilize the system not only locally but globally. This will involve solving a differential Riccati equation as opposed to the algebraic Riccati equation in the case of the LQR designed in Chapter 4. If we examine the system of ODEs (5.16) we notice that the heat transfer equation given by equation (5.3):

$$\rho C_v V_{SMA} \frac{d}{dt} T(t) = \frac{V^2}{R} - h A_{SMA} (T(t) - T_a), \quad (6.10)$$

does not depend on the space variable x , so the approach that we will be taking in the controller design is as follows; the heat transfer equation will be solved independently for the initial condition $T(0) = 270K$, and then substituted in the equation (5.16) relating stress and strain of the SMA. This results in a nonlinear ODE in the form:

$$\rho \frac{d^2}{dt^2} x(t) = \frac{\partial}{\partial x} \sigma(t) + u(t) + U_{control}(t), \quad (6.11)$$

where σ is given by equation (5.15), $T(t)$ is the solution of the heat equation (6.10) and is given by equation (6.12), $u(t)$ is the load function, and $U_{control}(t)$ is the control law. The function $T(t)$ is found using Maple's `dsolve` command for solving ODEs and it is given by:

$$T(t) = \frac{V^2}{h A_{SMA} R} + T_a + \exp \left[-\frac{h A_{SMA} t}{\rho V_{SMA} C_v} \right] \left(270 - \frac{V^2}{h A_{SMA} R} - T_a \right). \quad (6.12)$$

Let the desired trajectory, the reference input signal we would like the response of the SMA to follow, be a function $\tilde{x}(t)$, then the desired response of the nonlinear 1 DOF oscillator given by equation (6.11) is described by the following equation:

$$\rho \frac{d^2}{dt^2} \tilde{x}(t) = \frac{\partial}{\partial x} \tilde{\sigma}(t) + u(t) + \tilde{U}_{control}(t), \quad (6.13)$$

where $\tilde{U}_{control}(t)$ is a control function which maintains the SMA in the desired trajectory and $\tilde{\sigma}$ has the same expression as σ by substituting $\tilde{x}(t)$ for $x(t)$. If the function $\tilde{x}(t)$ is a solution of equation (6.11) without the control term then $\tilde{U}_{control}(t) = 0$.

Subtracting (6.13) from (6.11) and defining:

$$\vec{y} = \begin{bmatrix} x - \tilde{x} \\ \dot{x} - \dot{\tilde{x}} \end{bmatrix}, \quad (6.14)$$

where $\tilde{x}(t)$ is the desired trajectory and $x(t)$ is the trajectory of the nonlinear SMA described by equation (6.11) that we want to keep as close as possible to $\tilde{x}(t)$ by finding a suitable control law $U_{control}$. After substitution, and accounting for the damping effect with damping coefficient c_1 , the following system is obtained:

$$\begin{bmatrix} \dot{y}_1 \\ \dot{y}_2 \end{bmatrix} = \begin{bmatrix} y_2 \\ -\frac{c_1 y_2}{\rho} - \frac{k_1(T-T_M)y_1}{\rho} + \frac{k_2(y_1+\tilde{x})^3}{\rho} - \frac{k_2\tilde{x}^3}{\rho} - \frac{k_3(y_1+\tilde{x})^5}{\rho} + \frac{k_3\tilde{x}^5}{\rho} + \frac{\bar{U}}{\rho} \end{bmatrix}, \quad (6.15)$$

where $\bar{U} = U_{control}(t) - \tilde{U}(t)$ is the feedback control. Equation (6.15) has the form of equation (6.1), which can be reduced to the form of equation (6.3) after some algebraic manipulations:

$$\begin{aligned} \begin{bmatrix} \dot{y}_1 \\ \dot{y}_2 \end{bmatrix} &= \begin{bmatrix} 0 & 1 \\ -\frac{k_1}{\rho}(T-T_M) & -\frac{c_1}{\rho} \end{bmatrix} \begin{bmatrix} y_1 \\ y_2 \end{bmatrix} \\ &+ \begin{bmatrix} 0 & 0 \\ \frac{f(y_1, x_1)}{\rho} & 0 \end{bmatrix} \begin{bmatrix} y_1 \\ y_2 \end{bmatrix} + \begin{bmatrix} 0 \\ \frac{1}{\rho} \end{bmatrix} \bar{U}, \end{aligned} \quad (6.16)$$

where $f(y_1, x_1)$ is given by:

$$k_2(y_1 + \tilde{x})^2 + k_2(y_1 + \tilde{x})\tilde{x} + k_2\tilde{x}^2 - k_3(y_1 + \tilde{x})^3\tilde{x} - 4k_3\tilde{x}^4 - k_3\tilde{x}^2y_1^2 - 3k_3y_1\tilde{x}^3 - k_3(y_1 + \tilde{x})^4 + k_3\tilde{x}^4, \quad (6.17)$$

and from equations (6.16) and (6.3) the matrices A and B are given as follows:

$$A(t) = \begin{bmatrix} 0 & 1 \\ -\frac{k_1}{\rho} (T(t) - T_M) & -\frac{c_1}{\rho} \end{bmatrix}, \quad B = \begin{bmatrix} 0 \\ \frac{1}{\rho} \end{bmatrix}. \quad (6.18)$$

Example 1.

To demonstrate our approach in practice, let the desired trajectory be a periodic orbit: $\tilde{x} = \sin(10t) + \cos(5t)$.

By using the proposed feedback control design procedure (see equations (6.5)–(6.8)), we will demonstrate that the response of the chaotic motion of the SMA oscillator can be tracked to the desired periodic orbit by the optimal control law to be calculated next. The first step to finding the optimal control law given by (6.5) is to solve the Riccati equation given by (6.8) that requires matrix Q and the scalar R . As in the LQR controller design in Chapter 4, Q and R are chosen randomly [24, 39, 57]. We select Q and R as follows:

$$Q = \begin{bmatrix} 10 & 0 \\ 0 & 10 \end{bmatrix}, \quad B = \begin{bmatrix} 0 \\ \frac{1}{\rho} \end{bmatrix}, \quad \text{and } R = 0.001. \quad (6.19)$$

Next, we need to solve the differential Riccati equation (6.8), so let us define the matrix $P(t)$ as :

$$P(t) = \begin{bmatrix} P_{11}(t) & P_{12}(t) \\ P_{21}(t) & P_{22}(t) \end{bmatrix} \quad (6.20)$$

and substitute Q , R , $A(t)$, and B in equation (6.8), this results in a nonlinear system of ODEs (6.21) with the unknown functions are $P_{11}(t)$, $P_{12}(t)$, $P_{21}(t)$, and $P_{22}(t)$.

$$\begin{aligned}
\dot{P}_{11}(t) - \frac{P_{12}(t) k_1 (T(t) - T_M)}{\rho} - \frac{k_1 (T(t) - T_M) P_{21}(t)}{\rho} - 1000.0 \frac{P_{12}(t) P_{21}(t)}{\rho^2} + 10 &= 0, \\
\dot{P}_{21}(t) - \frac{P_{22}(t) k_1 (T(t) - T_M)}{\rho} + P_{11}(t) - \frac{c_1 P_{21}(t)}{\rho} - 1000.0 \frac{P_{22}(t) P_{21}(t)}{m^2} &= 0, \\
\dot{P}_{12}(t) + P_{11}(t) - \frac{P_{12}(t) c_1}{\rho} - \frac{P_{22}(t) k_1 (T(t) - T_M)}{\rho} - 1000.0 \frac{P_{12}(t) P_{22}(t)}{\rho^2} &= 0, \\
\dot{P}_{22}(t) + P_{21}(t) - 2 \frac{P_{22}(t) c_1}{\rho} + P_{12}(t) - 1000.0 \frac{(P_{22}(t))^2}{\rho^2} + 10 &= 0.
\end{aligned} \tag{6.21}$$

The system of ODEs given by (6.21) is solved for the functions P_{11} , P_{12} , P_{21} and P_{22} using Maple's numerical differential equation solver "dsolve" (for the corresponding Maple code see Appendix B). And by substituting B , R , and $P(t)$ in equation (6.5) we can conclude that the optimal control law $\bar{U}(t)$ has the following form:

$$\bar{U}(t) = -100y_1(t) P_{21}(t) - 100y_2(t) P_{22}(t). \tag{6.22}$$

Next, we substitute the optimal control law $\bar{U}(t)$ in equation (6.16) and solve the new system of ODEs for y_1 and y_2 to obtain the response of the closed-loop control system. The Figure 6.1 represents the response of the controlled nonlinear SMA oscillator system given by (6.16). By changing the reference input signal from an orbit to a sawtooth and then to a squarewave we can create several instructive examples where the response of the controlled SMA system does closely follow the reference input signal.

Example 2.

By changing the reference input signal to a sawtooth function using the following Maple command $f := x- > x - \text{floor}(x)$ and changing the parameter R value to

0.1, we get the response presented in Figure 6.2. From Figure 6.2 we observe that the response of the controlled SMA system does follow the reference input signal.

Example 3.

Finally, we will choose the reference signal as a squarewave and this time we be using

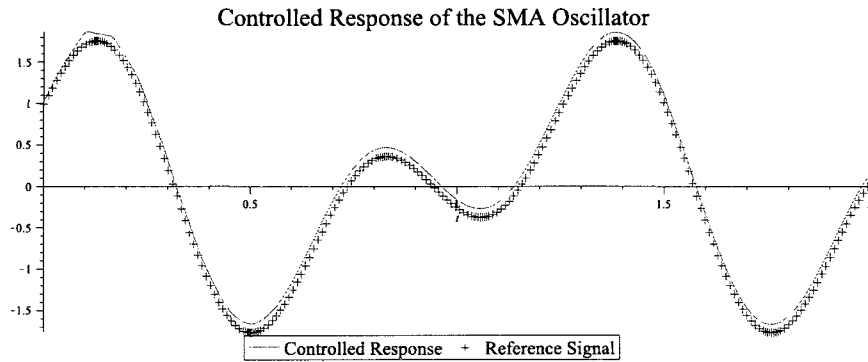


Figure 6.1: Periodic Orbit: Controlled Response of the Nonlinear Oscillator

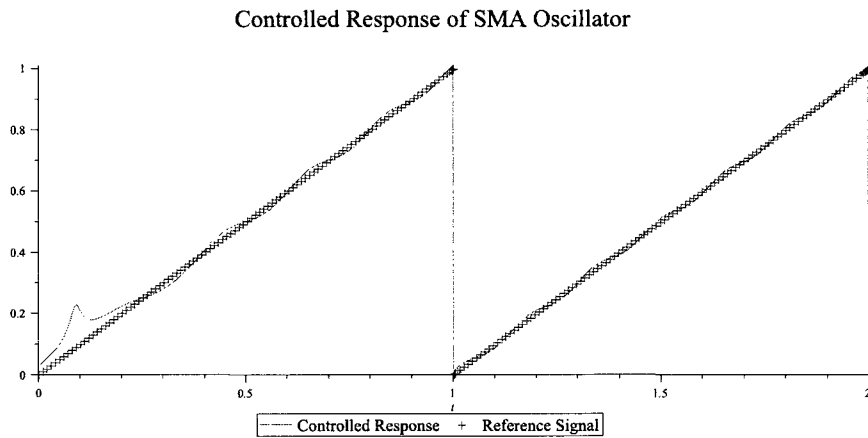


Figure 6.2: Sawtooth: Controlled Response of the Nonlinear Oscillator

the following Maple code:

$$\begin{aligned}
 f1(t) &= 2t - 2\text{floor}(t) - 1 \\
 f2(t) &= \text{abs}(2 * f1((2 * t - 1) * (1/4))) - 1 \\
 \text{SquareWave}(t) &= \text{signum}(f2(t))
 \end{aligned}
 \tag{6.23}$$

The response to a squarewave reference input signal is shown in Figure 6.3.

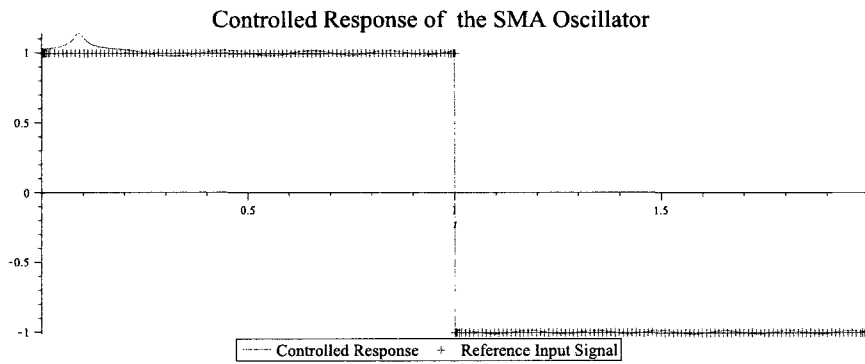


Figure 6.3: Squarewave: Controlled Response of the Nonlinear Oscillator

To control the SMA system presented in this chapter, one of the most challenging tasks is to determine the necessary inputs to drive the SMA system in a certain way, due to the existence of the hysteresis associated with the shape memory effects. From the results presented in the exercises above (see Figures 6.1–6.3), we can see that the designed controller, based on the linear control for nonlinear systems strategy, did indeed compensate for the hysteresis in the original dynamics of the system, and at the same time it drove the response of the SMA system in a desired manner by tracking a desired trajectory in the form of a reference input signal.

The stability of the closed-loop system given by equation (6.16) is guaranteed by way

of Lyapunov function as described by theorem 1. For dynamic systems similar to SMA systems, the Lyapunov function is always chosen as follows [39, 57]:

$$V(\vec{x}) = \vec{x}^T P(t) \vec{x}, \quad (6.24)$$

where $P(t)$ is a symmetric positive definite matrix that satisfies the Riccati equation (6.8). It can be shown that for positive definite matrices \tilde{Q} and R , the derivative of the function (6.24) is given by:

$$\dot{V}(\vec{x}) = -\vec{x}^T \tilde{Q} \vec{x} - \vec{u}^T R \vec{u}, \quad (6.25)$$

and, it is negative definite. Then, the function (6.24) is Lyapunov function, and the controlled system (6.16) is asymptotically stable.

6.3 Summary

In this chapter, optimal linear feedback control strategies for nonlinear systems were used to design a controller to stabilize the nonlinear SMA oscillator described by the system of equations (6.16). We applied the method in order to find a control law to eliminate the hysteresis in the SMA on the one hand, and to track the response of the SMA to a reference input signal on the other hand. Using the derived control law, the mathematical model of the closed-loop system was developed and simulated. The numerical results presented here were obtained using Maple's *RKF45* algorithm. The results show that the linear control design strategy applied to the nonlinear SMA system is effective in compensating for the hysteresis phenomenon and in linearizing the input/output relationship of the SMA system. Therefore, we can conclude that despite the inherent hysteresis nature of SMAs that hampered their usage in

many engineering applications, control methods, such as the one implemented in this chapter, can be applied to overcome the nonlinearities associated with the hysteresis phenomenon of SMAs, thus enabling SMAs to be used as a suitable source of actuation in many engineering applications.

Chapter 7

Conclusions

In this thesis, mathematical models for SMAs were developed to capture, analyze, and control their behavior. In the first part of the thesis, a 1 DOF nonlinear oscillator with a SMA element, in the form of a nonlinear spring, was used to study the nonlinear behavior of SMAs. The SMA spring in the nonlinear oscillator was used as an actuator that would exert a restoring force to pull mass m of the oscillator back to its initial position. Since SMAs exist in two distinct phases, martensite and austenite, we considered the case when the SMA existed in one of the phases by choosing the appropriate temperature. A mathematical model for the nonlinear oscillator with the SMA was then formulated for each phase, the model included the dynamics of the oscillator and the constitutive model describing the nonlinear behavior of the SMA. The behavior of the SMA was described by using the polynomial constitutive model that captures the main properties of SMAs. Each model was then simulated and computational results were presented. Due to the hysteretic nature of SMAs, the numerical results obtained showed that the response of the nonlinear oscillator

was chaotic and unpredictable, which hindered their effectiveness despite their unique properties. To overcome the difficulties related to hysteresis, a linear optimal control strategy was used to develop and implement a LQR controller to stabilize the nonlinear oscillator. The implementation of the LQR controller in a closed-loop feedback setup proved successful, and the numerical results showed that the chaotic response of SMAs can be eliminated, making SMA usage in many engineering applications feasible and desirable. The linear optimal control strategy has its limitations as it is based on system linearization, and the main limitation is the region of operation. To overcome this problem, in the second part of this thesis we considered a different approach. Recall that in the first part of this thesis we considered the SMA while it was in one of its two phases, martensite and austenite, and this was done by keeping the temperature constant. In the second part however, we did account for the coupling of the main physical quantities of continuum mechanics to the thermal field. A mathematical model describing the thermo-mechanical behavior of SMAs was developed using the conservation law of momentum and energy balance to model the dynamics of the SMA. The thermo-mechanical model was represented by a system of nonlinear PDE and ODE equations that do not have a general closed form solution. To overcome this problem, a model reduction based on the Galerkin method was used to transform the model from a system of nonlinear PDEs into a lower dimensional system of ODEs. The reduced model was then simulated and numerical results were presented. The results for the thermo-mechanical system showed that the response is chaotic and unpredictable, and prompted us to design an optimal controller that would eliminate or compensate for this behavior. This was achieved by choosing an optimal linear design for nonlinear systems to track the SMA's response. The con-

troller was successfully designed and implemented in a closed-loop feedback setup, and by using different input signals the numerical results show that the response of the controlled nonlinear oscillator was kept close to the reference input.

Appendices

Appendix A

Commercial SMAs and Their Applications

A.1 Commercial Shape Memory Alloys

A large number of SMAs have been discovered since the mid-1990s, and the list continues to grow. Many of these alloys, while scientifically interesting, consist of precious metals or only exhibit useful properties as single crystals, which do not lend them to practical use in commercial applications. Several groups of alloys, however, are commercially viable for novel devices and many others have strong potential. These include certain copper alloys and Ni-Ti-based alloys, such as near-equiatomic Ni-Ti, known as Nitinol¹ and some ternary alloys such as NiTiCu and NiTiNb. To date, it is fair to say that Ni-Ti-based SMAs have the best memory and superelasticity

¹Nitinol takes its name from Nickel-Titanium for its composition and NOL from Naval Ordnance Laboratory, which is the place where they first discovered its shape memory aspects

properties of all the known polycrystalline SMAs [18, 30, 69, 81].

A.1.1 Ni-Ti

Of all the shape memory alloys, Ni-Ti has been studied most extensively and has proven to be the most flexible and beneficial in engineering, biomedical, and scientific applications. Ni-Ti exhibits strong SME and pseudoelastic behavior, which makes it ideal for a variety of sensing and actuation applications. It also exhibits resistance to corrosion, greater ductility, more recoverable motion, the ability to be electrically heated for shape recovery, and high biocompatibility making it suitable for use in many biomedical applications [18, 20, 37]. The Ni-Ti Young's modulus for martensite is 21 to 69 GPa and austenite 70 to 110 GPa meaning austenite has a two to fourfold larger Young's modulus in comparison to martensite. SMAs can be activated by external heating or electrical heating. By electrical heating the energy consumption has to be considered carefully since most of the input energy is transformed to heat rather than mechanical strain resulting in low efficiency ($< 2\%$). The transformation temperature between low-temperature and high-temperature phase -200°C to 110°C can be adjusted by varying the proportions between nickel and titanium within the alloy [46] (and references therein). The equiatomic composition (i.e. 50% of Ni and Ti) exhibits the maximum A_f temperature (120°C) of all Ni-Ti compositions studied. Decreasing the Ni atomic percentage from the equiatomic composition does not change the transformation temperatures. If the composition of nickel is increased above 50%, the transformation temperature begins to decrease, with A_f becoming as low as -40°C for 51% nickel. This variation in composition can change

the ambient room temperature (23°C) characteristics from SME to pseudoelasticity. Recent studies have also investigated 55% Ni-Ti composition. This composition exhibits transformation temperatures in the range of -10°C to 60°C . The alloy is a chemically multi-phased alloy, which is one of the primary reasons why it exhibits low transformation strains. However, 55% Ni-Ti alloy has been proven to show superior corrosion resistance as compared to stainless steels in harsh environments such as a salt water bath or salt fog [30] (and references therein). Ni-Ti alloys are available as wires, rods, strips, plates, tubes, ribbons, and thin sheets.

A.1.2 Ni-Ti-Cu

Although Ni-Ti is the most common standard shape memory alloy available some of its properties might not be adept for specific designs, especially when used at high temperature. Because of this, extensive research has been conducted to improve some of its mechanical and thermal properties. One of the methods of doing this is by adding a ternary element to Ni-Ti, such as copper (Cu), zinc (Zn), iron (Fe), or aluminum (Al) [30, 81]. Adding a third elements opens even more possibilities for adapting binary NiTi alloys to more specific needs of applications [69]. The addition of Cu to Ni-Ti for example, forms the Ni-Ti-Cu alloy. Copper-based SMAs have some advantages, such as low cost and simple fabrication procedure, compared to TiNi alloys. Of the alloys, the ternary Cu-Zn-Al and Cu-Al-Ni alloys have been extensively studied and they are commercially available [81]. The unique property of these alloys is that addition of Cu reduces the hysteresis of the SMA response and lowers the martensite phase yield strength of the material compared to Ni-Ti [30]. Lower yield

strength on the martensite phase will decrease the amount of force required to deform the SMA element in that phase thus providing a higher net output force. The smaller temperature hysteresis provides faster actuation times or cycle rates, it can also make the actuator more suitable for thermal actuation [18]. However, copper-based alloys Cu based SMAs such as Cu-Al-Ni and Cu-Zn-Al suffer from low strength and poor corrosion resistance [81]. The material parameters of Ni-Ti as well as other SMAs are listed in Table A.2.

A.1.3 Au-Cu-Zn

Au-Cu-Zn alloy is also known as superelastic dental Au-Cu-Zn as it finds its use in dentistry. Au is an element that is important to improve corrosion resistance in the oral mouth and bring about a superelastic effect with Cu and Zn. Cu is an element that is necessary to limit melting point of alloys to a relatively low value and increase the tensile strength and elongation thereof. However, as the amount of Cu increases, there is a tendency for the superelastic effect toward dropping. On the other hand, as the amount of Cu decreases, the resulting alloys have an increased melting point. Zn is an element that combines a deoxidation with castability-improving effect. However, the amount of Zn decreases, there is a tendency for superelastic effect toward dropping, whereas as the amount of Zn increases, there is a lowering of tensile strength and elongation. The superelastic dental Au-Cu-Zn alloys are easily formed into dental cast materials with good precision by means of the conventional dental precision casting process. These alloys are free from any toxicity in the oral mouth, excel in corrosion resistance, and have excellent durability [84].

A.1.4 Ni-Mn-Ga

Another type of SMAs that is becoming popular in the research arena is the Magnetic Shape Memory Alloys (MSMAs). These type of SMAs alloys present the same properties as the classic SMAs but with the addition of a magnetic field sensibility. The interest in MSMAs stems from their possible activation not only by stress and temperature actions but also by magnetic field [19, 30]. The magnetoelastic martensitic transformation in MSMAs is defined as: when a magnetic field is applied to an alloy that exhibits a thermoelastic martensitic transformation, martensite variants may be induced while a magnetic field is applied and revert to the parent phase when the magnetic field is removed. The best known, and the most widely investigated MSMAs are Ni-Mn-Ga alloys [30], they have been shown to produce large strains of 6 to 10 % when exposed to magnetic fields of 400 to 640 kA/m, and actuator systems with these type of MSMAs typically achieve 2 to 3 % active strain [69]. While these strains are of the same order as those seen in shape memory alloys, the rotation of twin martensitic variants in response to magnetic activation is faster and thus can lead to faster response than those achieved through martensite-austenite phase transformations. Ni-Mn-Ga alloys have a field and strain dependent Young's modulus of 0.45 to 0.82 GPa. The density of the material is 8.36 g/cm³. Operating temperatures of Ni-Mn-Ga MSM materials presently ranges from -40°C to 60°C [46] (and references therein). Despite their unique properties and potential, MASMa have been difficult and expensive to make. More recently, researchers have produced a lighter and potentially cheaper MSMAs. This new material, a porous foam made from a Ni-Mn-Ga alloy, stretches slightly when exposed to a magnetic field. It retains its

new form when the field is turned off, but it goes back to its original shape when the field is rotated 90 degrees. Making the foam is cheap and easy. The researchers pour molten alloy into a porous piece of sodium aluminate salt. After the alloy cools, the researchers dissolve the salt using acid, leaving behind a spongelike structure of the alloy. This material, sometimes referred to as smart foam, could be useful in devices that need very precise, repeatable, and rapid positioning. These devices include microscopes, tiny mirrors used in optical communication, and robots used in medicine. Because the foam is light, it could also lead to aerospace applications [54].

A.1.5 Thin Film SMAs

More recently, thin film SMAs have been recognized as a new type of promising and high-performance material for microelectromechanical system (MEMS) [45]. Among these SMA films, Ti-Ni based films are the most promising ones. The main advantages for MEMS applications of Ti-Ni thin film include high power density, large displacement and actuation force and low operation voltage. Application of SMA films in MEMS also facilitates the simplification of mechanisms with flexibility in design and creation of clean, friction free and non-vibrating movement. In order to apply the Ti-Ni alloys to MEMS, it is required to make them thin down to micron sizes. Rolling and melts-pinning methods are available for making thin plates with thickness larger than 15 μm . However, sputter-deposition techniques are available for making thin films with thicknesses less than 10 μm . Ti-Ni thin films fabricated by the sputter-deposition method are expected to be applied to microdevices such as microvalves, micropumps and cantilevers, since they exhibit an excellent shape

memory effect and good mechanical properties [45].

A.1.6 Porous SMAs

Porous SMAs have also attracted increasing attention for possible applications in medical implant devices and as high energy absorption structural material. The progress in manufacturing and characterization of the porous Ni-Ti SMA has been reported by a number of researchers [85] (and references therein). Different fabrication techniques for producing porous SMAs have been established. Some techniques focus on injecting gas into a melt, but most of the research work done on porous SMAs has been focused on using powder metallurgy techniques [14]. The authors in [85] for example, produced porous Ni-Ti using Ni-Ti powder using the Spark Plasma Sintering (SPS) technique, examples of porous SMAs with different volume percentages are given in Table A.1. Porous SMAs have a great potential application in orthopedic implants since their porosity enables the transport of body fluids from outside to inside the bone, which is important in the healing process. This fact optimizes the treatment and also helps the fixation of the implant [37]. Another application where porous SMAs can play a significant role ranges from isolation of machines and equipment to isolation of payloads during launch of space vehicles [14].

A.2 Shape Memory Alloys Applications

The unique properties of SMA have prompted researchers and engineers to incorporate them in various applications in different fields of engineering. SMAs have been utilized in military, medical, micro-robotics, as well as other applications. In this

Table A.1: Ni-Ti Specimens Processed by Spark Plasma Sintering [85]

| Name of sample | Porosity | SPS Processing Conditions | Transformation Temperature (°C) |
|------------------|----------|---------------------------|--|
| Dense Ni-Ti | 0 | 850°C under 50 MPa, 5min | $A_s = 23.88, A_f = 43.12$ $M_s = 36.05, M_f = 23.09$ |
| 13% porous Ni-Ti | 13% | 800°C under 25 MPa, 5min | $A_s = 19.3, A_f = 38.82$ $M_s = 20.65, M_f = 5.39$ |
| 25% porous Ni-Ti | 25% | 750°C under 5 MPa, 5min | $A_s = 14.59, A_f = 33.29$ $M_s = 23.24, M_f = 2.55$ |

Table A.2: Properties of Different SMAs [48]

| Item | Ni-Ti | Cu-Zn-Al | Cu-Al-Ni | Ni-Mn-Ga | Ni-Ti-Cu |
|---------------------------------|----------|----------|----------|----------------------|----------|
| Density (Kg/cm^3) | 6450 | 7900 | 7150 | $8.36 \cdot 10^{-3}$ | 6500 |
| Young Modulus (GPa) | 30-70 | 70-100 | 80-100 | 0.45-0.82 | 25-50 |
| Transformation Temperature (°C) | -100-110 | -200-110 | -250-200 | -40-60 | -140-250 |

section we present a discussion of some applications of SMAs.

A.2.1 Medical Applications

In recent years, medicine and the medical industry have focused on the concept of less invasive surgical procedures. Following this tendency, shape memory surgical instruments have been created and are becoming noticeable. SMA biomedical applications have become successful due to the noninvasive characteristic of SMA devices and also due to their excellent biocompatibility². In [37], the author discussed a number of medical applications where SMAs played a significant role in designing medical devices. SMAs are usually employed in surgical instruments, cardiovascular, orthopedic, and orthodontic devices, among other applications.

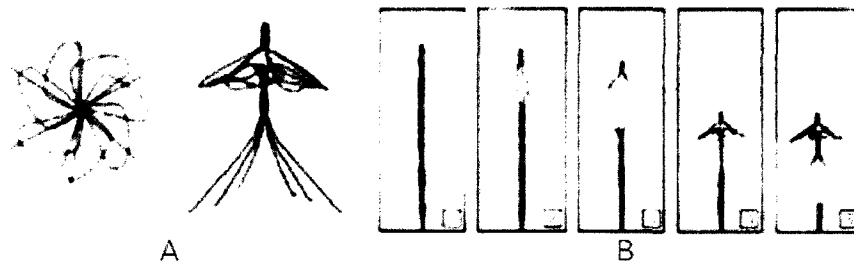


Figure A.1: Simon Filter, taken from www.nitinol.com with permission, courtesy of NDC

²Biocompatibility is the ability of a material to remain biologically innocuous during its functional period inside a living creature. This is a crucial factor for the use of SMA devices in the human body. A biocompatible material does not produce allergic reactions inside the host, and also does not release ions into the bloodstream. The period during which a biomaterial remains inside the human body is an important aspect to be considered concerning its use.

In cardiology for example, the first cardiovascular device developed with a SMA was the Simon filter. The Simon filter Figure A.1 represents a new generation of devices that are used for blood vessel interruption in order to prevent pulmonary embolism. Persons who cannot take anticoagulant medicines are the major users of the Simon filter. The purpose of this device is to filter clots that travel inside the bloodstream. The Simon filter traps these clots that in time are dissolved by the bloodstream. The insertion of the filter inside the human body is done by exploiting the shape memory effect. From its original shape in the martensitic state Figure A.1 the filter is deformed and placed on a catheter tip. Saline solution flowing through the catheter is used to keep a low temperature, while the filter is placed inside the body. When the catheter releases the filter, the flow of the saline solution is stopped. As a result, the bloodstream promotes the heating of the filter that returns to its former shape. In orthopaedy, SMAs have been used to make vertebra spacer. The insertion of this spacer between two vertebrae assures the local reinforcement of the spinal vertebrae, preventing any traumatic motion during the healing process. The use of a shape memory spacer permits the application of a constant load regardless of the position of the patient, who preserves some degree of motion. This device is used in the treatment of scoliosis . Figure A.2 shows spinal vertebrae and a shape memory spacer. On the left side, the spacer is in the martensitic state, and on the right side, the spacer is in its original shape, recovered by the pseudo-elastic phenomenon.

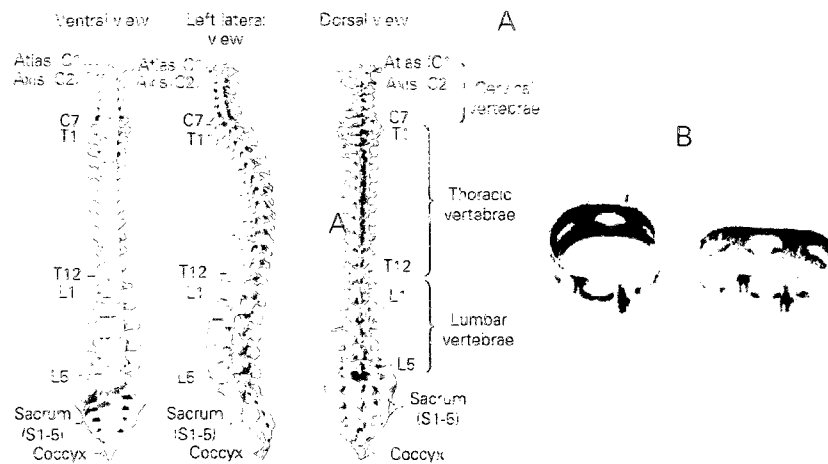


Figure A.2: Spinal vertebrae (A) and shape memory spacers (B) in the martensitic state (left) and in the original shape (right). Taken from [37] with permission.

A.2.2 SMAs in Dentistry

SMAs have also found their use in dentistry due to their remarkable biocompatibility, durability, corrosion resistance, and superelasticity. In orthodontics for example, see Figure A.3, SMAs have been used as archwires to move teeth with light continuous force. SMA archwires play a significant role in the alignment and leveling of teeth. The SMA used in this application is thermally activated and is fully martensitic at room temperature. The austenitic finish temperature of these wires is at approximately 32°C , which ensures that the wire is fully transformed at body temperature [86].

A.2.3 Robotics

Another area where SMAs have been used is humanoid robotics. In the years 2006 and 2007 at the Darmstadt University of Technology, a female robot by the name of Lara was built, and was actuated by 34 SMA actuators. To use SMA as an actuator for humanoid robots high forces are needed, but the cycle time highly increases with the wire's diameter. To avoid this property the new actuator/sensor were made by combining many single SMA wires in a new way to one muscle-like actuator. Using two of these actuators in an antagonistic flexor-extensor muscle-like manner offers the possibility to generate a defined force at every time. The pull force depends directly on the number of wires. One type of actuator used in the humanoid robot was made up of 10 pairs of SMA wires with a thickness of 100 micrometer and 180 gf pull-force each. The total pull force is 3.6 kgf. The actuator has a length of 22 cm and a maximal displacement of 1.5 cm. The humanoid hand shown in Figure A.4 consisted of 5 fingers and was actuated by 7 SMA actuators and several springs [28].

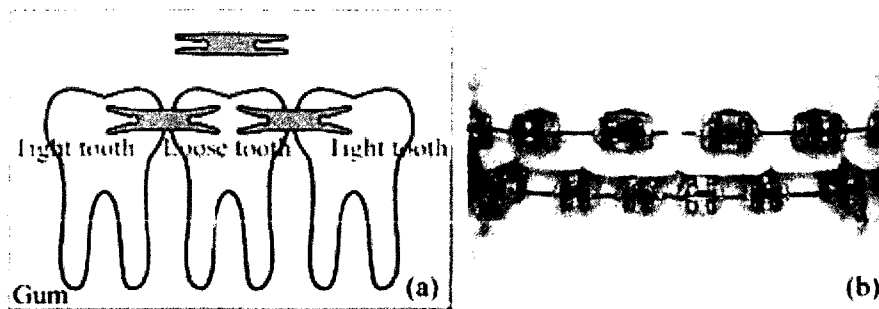


Figure A.3: Dental Applications of Ni-Ti, taken from <http://www.keytometals.com> with permission

[28]

A.2.4 Space Application

SMA's have also been used in a number of space applications. They have been used as actuators, since their large power density offers compact and lightweight solutions, and their operation involves low accelerations and low voltage. SMA actuators have successfully been applied on spacecraft in release and unfolding mechanisms for solar panels, such as those of the Hubble Space Telescope as well as new microsattellites [31]. In [2] for example, the authors gave a detailed account of how the Air Force Research Laboratory (AFRL), with corporate and government partners, has developed SMA spacecraft release mechanisms and hinges as alternatives to current off-the-shelf devices that may not be able to meet future satellite requirements. SMA-based systems are also being developed for the deployment of antennae, satellite, and inflatable structures in space programs. In [55] for instance, the authors discuss how SMA actuators were used to develop a large surface area to mass ratio inflatable space structure with possible applications for a synthetic radar aperture (SAR) antenna. The key components of this inflatable structure are inflatable tubes, membrane, and the links installed in-between stretching the membrane as seen in Figure A.5. The SMA actuators are installed in series with the links, which realize the tensions according to the



Figure A.4: Humanoid Robot Hand [28], taken from <http://www.lararobot.de> with permission

instructions from a control system.

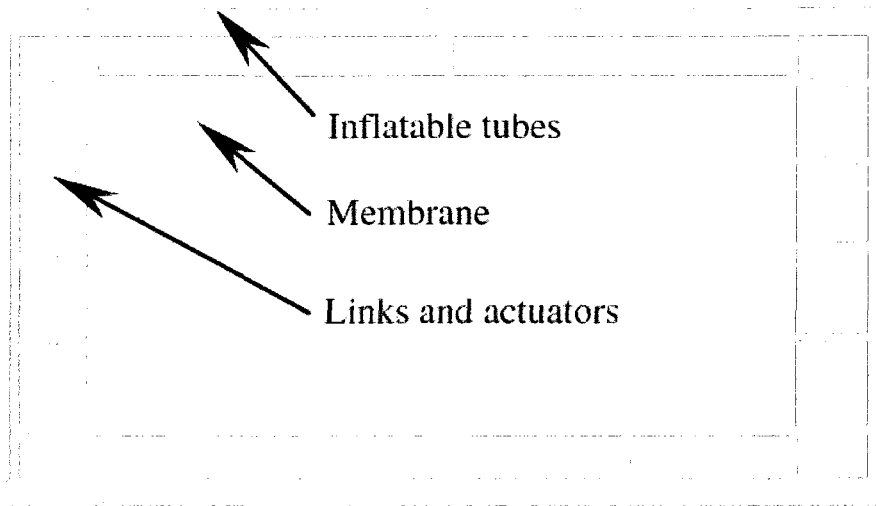


Figure A.5: Sketch of the inflatable structure [55]

A.2.5 SMA Micro-Damper for Microelectromechanical (MEMS)

Applications

There is an ever increasing demand for miniaturize devices, such as micro-dampers and micro-sensors, that are finding increased use in portable and mobile electronic and mechanical systems. SMAs are receiving special attentions for the MEMS systems applications nowadays. In [61], the authors proposes a Ni-Ti wire base micro-damper, see Figure A.6, utilizing the pseudoelasticity behavior of SMAs. The main components of the micro-damper consist of internal shaft, external tube, blocks, shims, springs, slippers and NiTi wires. The length of the damper is designed as 32mm and the diameter is 14mm for special study purpose here. The diameter of Ni-Ti wires is

0.14mm and its free length is 35mm.

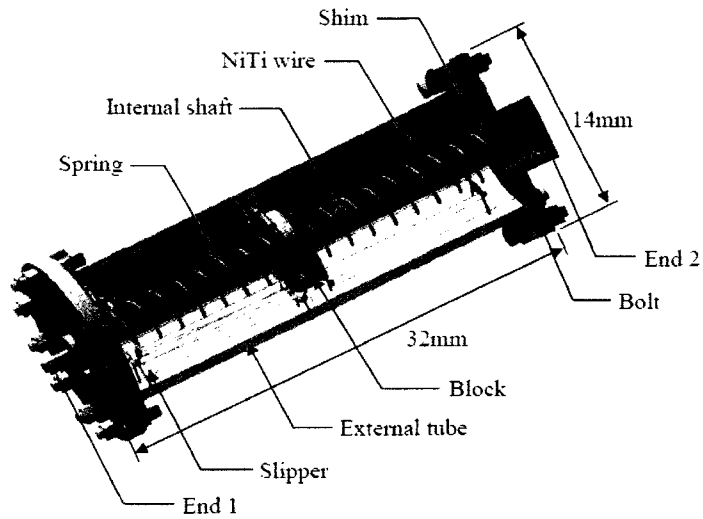


Figure A.6: Prototype of SMA Micro-Damper [61]. Permission granted for noncommercial purposes, courtesy of MDPI (www.mdpi.org).

Appendix B

Maple Routines

B.1 Numerical simulation

Maple is a technical computing software that has a large library of built-in functions that allows users to solve a large number of engineering problems. One of the areas where Maple is useful is for solving differential equations as well as partial differential equations numerically and symbolically. It also has a large set of plotting and graphing routines for creating 2D and 3D plots and many other types of plots.

In this thesis Maple is used to do all the simulations and the routines that were used are listed in this appendix.

The equation of motion that governs the vibrating 1 DOF nonlinear oscillator is a second order nonlinear differential equation, where $x(t)$ is the displacement of mass m and $u(t)$ is the input signal. Maple's numeric `dsolve` command is used to solve the ODE and the results are plotted using Maple's plotting routines.

$$m \frac{d^2}{dt^2} x(t) + c \frac{d}{dt} x(t) + a(T - T_M) x(t) - b(x(t))^3 + \frac{4b^2(x(t))^5}{a(T_A - T_M)} = u(t) \quad (\text{B.1})$$

```
params := [a = 1, b = 0.40e5, T_M = 287, T_A = 364, T = 283, c = .2]
```

```
ode := eval(ode1, [u(t) = 5 * sin(10 * t), params[]])
```

```
ics := x(0) = .1, (D(x))(0) = 0
```

```
sol := dsolve([ode, ics], numeric)
```

```
plots[odeplot](sol, [t, x(t)], t = 0..10, numpoints = 3000)
```

B.2 Controllability

The Maple routine `ControllabilityMatrix` computes the Controllability matrix

$$C = \begin{pmatrix} B & A \times B & A^2 \times B & \dots & A^{n-1} \times B \end{pmatrix} \quad (\text{B.2})$$

where A is an $n \times n$ matrix and B is an $n \times m$ matrix

```
ControllabilityMatrix:=proc(A::Matrix,B::Vector)
```

```
local i,nA,mA,nB,mB,C,G;
```

```
G := Matrix(B);
```

```
(nA, mA) := op(1, A);
```

```
(nB, mB) := op(1, G);
```

```
if nA <> mA then
```

```
error "first matrix must be square"
```

```
elif nB <> nA then
```

```
error "input matrices must have same row dimension";
```

```
else
```

```

G := LinearAlgebra : -LA_Main : -MatrixMatrixMultiply(A, G, inplace = false, outputoptions :
[]);
C := Matrix(nB, nB * mB, datatype = rtable_options(G, datatype));
C[1..nB, 1..mB] := B;
C[1..nB, mB + 1..2 * mB] := G;
for i from 2 to (nB - 1) do
G := LinearAlgebra : -LA_Main : -MatrixMatrixMultiply(
A, G, inplace = false, outputoptions = []);
C[1..nB, i * mB + 1..(i + 1) * mB] := G;
od;
fi;
return C;
end:

```

B.3 Observability

The Maple routine `ObservabilityMatrix` computes the observability matrix

$$O = \begin{pmatrix} C \\ C \times A \\ C \times A^2 \\ \vdots \\ C \times A^{n-1} \end{pmatrix} \quad (\text{B.3})$$

where A is an $n * n$ matrix and B is an $m * n$ matrix.

```
ObservabilityMatrix:=proc(A::Matrix,C::Vector)
```

```
local i,nA,mA,nC,mC,O,G;
```

```
G := Matrix(C);
```

```
(nA,mA):=op(1,A);
```

```
(nC,mC):=op(1,G);
```

```
if nA <> mA then
```

```
error "first matrix must be square"
```

```
elif mC <> mA then
```

```
error "input matrices must have same column dimension";
```

```
else
```

```
Linear Algebra : - $LA_{Main}$  : -MatrixMatrixMultiply(G, A, inplace = true, outputoptions = []);
```

```
O := Matrix(nC * mC, mC, datatype = rtable_options(G, datatype));
```

```
O[1..nC, 1..mC] := C;
```

```
O[nC + 1..2 * nC, 1..mC] := G;
```

```
for i from 2 to (mC-1) do
```

```
Linear Algebra : - $LA_{Main}$  : -MatrixMatrixMultiply(
```

```
G, A, inplace = true, outputoptions = []);
```

```
O[i * nC + 1..(i + 1) * nC, 1..mC] := G;
```

```
od;
```

```
fi;
```

```
return O;
```

```
end;
```

B.4 LQR Control

```
LQRControl := proc(A :: Matrix(numeric),  
B :: Matrix(numeric),  
Q :: Matrix(numeric),  
R)  
  
    local i, n, invR, ham, evals, evecs, M1, M2, j, k, K, P, output_type;  
  
    n := op([1, 1], A); RowDimension(A)  
  
    if type(R, 'Matrix(numeric)') then  
invR := LinearAlgebra : -MatrixInverse(R);  
    elif type(R, 'numeric') then  
invR := Matrix([[1/R]]);  
    else  
error "%-1 parameter must be of type numeric"  
"or a matrix with numeric entries", 4;  
    fi;  
  
    output_type := LinearAlgebra : -GetResultDataType(  
rtable_options(A, 'datatype'),  
rtable_options(B, 'datatype'),  
UseHardwareFloats);
```

```

form the Hamiltonian matrix

ham := Matrix([[A, -B.invR.LinearAlgebra : -Transpose(B)],
[-Q, -LinearAlgebra : -Transpose(A)]],
'datatype' = output_type);

(evals, evecs) := LinearAlgebra : -Eigenvectors(ham);

M1 := Matrix(n, n);
M2 := Matrix(n, n);

j := 0;
for i from 1 to 2*n do
if Re(evals[i]) < 0 then
j := j + 1;
for k from 1 to n do
M1k,j := evecsk,i;
M2k,j := evecsn+k,i;
od;
fi;
od;

P := map(Re, M2.LinearAlgebra : -MatrixInverse(M1));
K := invR.LinearAlgebra : -Transpose(B).P;

```

end;

Bibliography

- [1] A. A. Alonso, C. V. Fernandez, and J. R. Banga. DISSIPATIVE SYSTEMS: FROM PHYSICS TO ROBUST NONLINEAR CONTROL. *International Journal of Robust and Nonlinear Control*, 14:157–179, 2004.
- [2] B. C. Andrew Peffer, Eugene Fosnessb and K. Denoyer. ON-ORBIT EXPERIMENTS AND APPLICATIONS OF SHAPE MEMORY ALLOY MECHANISMS. *Proceedings of SPIE*, 3991:187–194, 2000.
- [3] A. Antonios and P. D. Christofides. FINITE-DIMENSIONAL CONTROL OF NON-LINEAR PARABOLIC PDE SYSTEMS WITH TIME-DEPENDENT SPATIAL DOMAINS USING EMPIRICAL EIGENFUNCTIONS. *International Journal of Applied Mathematics and Computer Science*, 11(2):287–317, 2001.
- [4] F. Borrelli and T. Keviczky. DISTRIBUTED LQR DESIGN FOR IDENTICAL DYNAMICALLY DECOUPLED SYSTEMS. Technical report, University of Minnesota, 2006.
- [5] L. C. Brinson. FINITE EEELEMENT ANALYSIS OF THE BEHAVIOR OF SHAPE MEMORY ALLOYS AND THEIR APPLICATIONS. *Solid Structures*, 30:3261–3280, 1992.

- [6] L. C. Brinson and R. Lammering. ONE DIMENSIONAL CONSTITUTIVE BEHAVIOR OF SHAPE MEMORY ALLOYS: THERMOMECHANICAL DERIVATION WITH NON-CONSTANT MATERIAL FUNCTIONS AND REDEFINED MARTENSITE INTERNAL VARIABLES. *Intelligent Material Systems and Structures*, 4:229–242, 1993.
- [7] B. Brogliato. DISSIPATIVE SYSTEMS ANALYSIS AND CONTROL. Springer, 2007.
- [8] A. Chatterjee. AN INTRODUCTION TO THE PROPER ORTHOGONAL DECOMPOSITION. *Current Science*, 78(7):808–817, 2000.
- [9] C. T. Chen. LINEAR SYSTEM: THEORY AND DESIGN. Oxford University Press, 1999.
- [10] L. Debnath and P. Mikusinski. INTRODUCTION TO HILBERT SPACES WITH APPLICATIONS. *Journal of the American Statistical Association*, 94(448):1390, 1999.
- [11] B. T. Dickinson and J. R. Singlerf. NONLINEAR MODEL REDUCTION USING GROUP PROPER ORTHOGONAL DECOMPOSITION. *International Journal of Numerical Analysis and Modeling*, 7(2):356–372, 2010.
- [12] C. Dickinson and J. Wen. FEEDBACK CONTROL USING SHAPE MEMORY ALLOY ACTUATORS. *Journal of Intelligent Material Systems and Structures*, 9:242–243, 1998.
- [13] M. Elahinia. NONLINEAR CONTROL OF A SHAPE MEMORY ALLOY ACTUATED MANIPULATOR. Master’s thesis, Rose School, European School of Advanced Studies in Reduction of Seismic Risk, September 2003.

- [14] P. B. Entchev. *Micromechanical Modeling of Porous Shape Memory Alloys*. PhD thesis, Texas A&M University, May 2002.
- [15] F. Falk. MODEL FREE ENERGY, MECHANICS, AND THERMODYNAMICS OF SHAPE MEMORY ALLOYS. *Acta Metallurgica*, 28:1773–1780, 1980.
- [16] F. Falk. LANDAU THEORY AND MARTENSITIC PHASE TRANSITIONS. *Le Journal de Physique Colloques*, 43(C4):3–15, 1982.
- [17] R. A. Freeman and P. V. Kokotovic. *ROBUST NONLINEAR CONTROL DESIGN*. Birkhauser, 1996.
- [18] D. Fugaza. SHAPE MEMORY ALLOY DEVICES IN EARTHQUAKE ENGINEERING: MECHANICAL PROPERTIES, CONSTITUTIVE MODELING AND NUMERICAL SIMULATION. Master’s thesis, Villanova University, Pennsylvania, August 2001.
- [19] J. Gauthier, C. LExcellent, a. Hubert, J. Abadie, and N. Chaillet. NI-MN-GA SINGLE CRYSTAL SHAPE MEMORY ALLOY MAGNETO-THERMOMECHANICAL MODELING. *EPJ Web of Conferences*, 6:29003, 2010.
- [20] X. Gong and A. R. Pelton. FINITE ELEMENT ANALYSIS ON NITINOL MEDICAL APPLICATIONS. In *International Mechanical Engineering Congress & Exposition*, pages 1–9, New Orleans, Louisiana, 2002.
- [21] R. B. Gorbet and D. W. L. Wang. A DISSIPATIVITY APPROACH TO STABILITY OF A SHAPE MEMORY ALLOY POSITION CONTROL SYSTEM. *IEEE Transactions on Control Systems*, 6:554–562, 2002.

- [22] W. M. Haddad and Q. Hui. DISSIPATIVITY THEORY FOR DISCONTINUOUS DYNAMICAL SYSTEMS: BASIC INPUT, STATE, AND OUTPUT PROPERTIES, AND FINITE-TIME STABILITY OF FEEDBACK INTERCONNECTIONS. *Nonlinear Analysis: Hybrid Systems*, 3:551–564, 2009.
- [23] J. P. Hespana. LECTURE NOTES ON LQR/LQG CONTROLLER DESIGN. <http://www.ece.ucsb.edu/roy/classnotes/147c/lqrlqgnotes.pdf>, April 2007.
- [24] J. Jayender, R. Patel, S. Nikumb, and M. Ostojic. MODELING AND CONTROL OF SHAPE MEMORY ALLOY ACTUATORS. *IEEE Transactions on Control Systems Technology*, 16(2):279–287, 2008.
- [25] H. K. Khalil. NONLINEAR SYSTEMS. Prentice Hall, 1996.
- [26] D. E. Kirk. OPTIMAL CONTROL THEORY, AN INTRODUCTION. Dover Publications, 2004.
- [27] D. Kovacs. INERTIAL MANIFOLDS AND NONLINEAR GALERKIN METHODS. Master’s thesis, Virginia Polytechnic Institute and State University, December 2005.
- [28] R. Kratz. THE LARA PROJECT. <http://www.lararobot.de/>, 2008.
- [29] K. Kunisch, S. Volkwein, and L. Xie. HJB-POD-BASED FEEDBACK DESIGN FOR THE OPTIMAL CONTROL OF EVOLUTION PROBLEMS. *SIAM Journal of Applied Dynamical Systems*, 3(4):701–722, 2004.
- [30] D. C. Lagoudas. SHAPE MEMORY ALLOYS: MODELING AND ENGINEERING APPLICATIONS. Springer, 2008.

- [31] M. Langelaar, G. H. Yoon, S. Gurav, Y. Y. Kim, and F. van Keulen. ANALYSIS AND DESIGN TECHNIQUES FOR SHAPE MEMORY ALLOY MICROACTUATORS FOR SPACE APPLICATIONS. <https://escies.org/GetFile?rsrcid=1703>, 2004.
- [32] C. J. Lee and C. Mavroidis. ANALYTICAL DYNAMIC MODEL AND EXPERIMENTAL ROBUST AND OPTIMAL CONTROL OF SHAPE-MEMORY-ALLOY BUNDLE ACTUATORS. www.robots.rutgers.edu/papers/IMECE2002.1.pdf, 2002.
- [33] W. S. Levine. THE CONTROL HANDBOOK. CRC Press and IEEE Press, 1999.
- [34] F. L. Lewis. OPTIMAL CONTROL. John-Wiley, 1986.
- [35] C. Liang and C. A. Rogers. ONE-DIMENSIONAL THERMOMECHANICAL CONSTITUTIVE RELATIONS FOR SHAPE MEMORY MATERIALS. *Journal of Intelligent Material Systems and Structures*, 2:207–234, 2004.
- [36] L. Machado. SHAPE MEMORY ALLOYS FOR VIBRATION ISOLATION AND DAMPING. Master’s thesis, Texas A & M University, December 2007.
- [37] L. G. Machado and M. A. Savi. MEDICAL APPLICATIONS OF SHAPE MEMORY ALLOYS. *Brazilian Journal of Medical and Biological Research*, 36(6):683–91, 2003.
- [38] L. G. Machado and M. C. Savi. AN OVERVIEW OF CONSTITUTIVE MODELS FOR SHAPE MEMORY ALLOYS. *Brazilian Journal Of Medical And Biological Research*, 36:1–31, 2006.
- [39] J. M. B. Marat Rafikov and A. M. Tusset. AN OPTIMAL LINEAR CONTROL DE-

- SIGN FOR NONLINEAR SYSTEMS. *Journal of the Brazilian Society of Mechanical Sciences and Engineering*, 30(4):279–284, 2008.
- [40] C. Mavroidis. DEVELOPMENT OF ADVANCED ACTUATORS USING SHAPE MEMORY ALLOYS AND ELECTORRHEOLOGICAL FLUIDS. *Research in Nondestructive Evaluation*, 14:1–32, 2002.
- [41] R. Melnik. ON CONSISTENT REGULARITIES OF CONTROL AND VALUE FUNCTIONS. *Numerical Functional Analysis and optimization*, 18(3 & 4):410–426, 1997.
- [42] R. Melnik. MARKOV CHAIN NETWORK TRAINING AND CONSERVATION LAW APPROXIMATIONS: LINKING MICROSCOPIC AND MACROSCOPIC MODELS FOR EVOLUTION. *Applied Mathematics and Computation*, 199(1):315–333, 2008.
- [43] R. Melnik and A. Roberts. MODELLING NONLINEAR DYNAMICS OF SHAPE-MEMORY-ALLOYS WITH APPROXIMATE MODELS OF COUPLED THERMOELASTICITY. *ZAMM*, 83(2):93–104, 2003.
- [44] R. V. N. Melnik. DETERMINISTIC AND STOCHASTIC DYNAMICS WITH HYPERBOLIC HJB-TYPE EQUATIONS. *Dynamics of continuous discrete and impulsive systems series A: Mathematical Analysis*, 10(1–3):510–520, 2003.
- [45] S. Miyazaki, Y. Fu, and W. Huang. THIN FILM SHAPE MEMORY ALLOYS FUNDAMENTALS AND DEVICE APPLICATIONS. Cambridge University Press, 2009.
- [46] H. P. Mooner. SMART MATERIALS FOR ACTIVE NOISE AND VIBRATION RE-

- DUCTION. In *Novem - Noise and Vibration: Emerging Methods*, pages 18–21, Sain-Raphael, France, 2005.
- [47] C. Navasca and A. Krener. SOLUTION OF HAMILTON-JACOBI-BELLMAN EQUATIONS. In *Proceedings of the 39th IEEE Conference on, Decision and Control, 2000*, volume 1, pages 570–574, Sydney, NSW, 2002. IEEE.
- [48] M. Novotny. SHAPE MEMORY ALLOYS: METALLURGY, BIOCOMPATIBILITY, AND BIOMECHANICS FOR NEUROSURGICAL APPLICATIONS. *Neurosurgery*, 64(5):199–214, 2009.
- [49] K. T. Oner, E. Cetinsoy, E. Sirimoglu, C. Hancer, T. Ayken, and M. Unel. LQR AND SMC STABILIZATION OF A NEW UNMANNED AERIAL VEHICLE. *Engineering and Technology*, 58:373–378, 2009.
- [50] K. Otsuka and X. Ren. PHYSICAL METALLURGY OF TI-NI BASED SHAPE MEMORY ALLOYS. *Progress in Materials Science*, 50:511–678, 2005.
- [51] E. Ott. CHAOS IN DYNAMICAL SYSTEMS. Cambridge University Press, 2002.
- [52] Y. Ou and E. Schuster. MODEL PREDICTIVE CONTROL: TERMINAL REGION AND TERMINAL WEIGHTING MATRIX. *Journal of Systems and Control Engineering*, 222(2):69–79, 2008.
- [53] A. Paiva and M. A. Savi. AN OVERVIEW OF CONSTITUTIVE MODELS FOR SHAPE MEMORY ALLOYS. *Mathematical Problems in Engineering*, 2006:1–31, 2006.
- [54] P. Patel. SMART FOAM. <http://www.technologyreview.com/communications/20016/page1/>, YEAR = 2008.

- [55] F. Peng, X. Jiang, Y. Hu, and A. Ng. ACTUATION PRECISION CONTROL OF SMA ACTUATORS USED FOR SHAPE CONTROL OF INFLATABLE SAR ANTENNA. *Acta Astronautica*, 63:578–585, 2008.
- [56] C. Pfeiffer, K. DeLaurentis, and C. Mavroidis. SHAPE MEMORY ALLOY ACTUATED ROBOT PROSTHESES: INITIAL EXPERIMENTS. In *Proceedings 1999 IEEE International Conference on Robotics and Automation*, pages 2385–2391. IEEE, 1999.
- [57] V. Piccirillo and J. M. Balthazar. CHAOS CONTROL OF A NONLINEAR OSCILLATOR WITH SHAPE MEMORY ALLOY USING AN OPTIMAL LINEAR CONTROL: PART I: IDEAL ENERGY SOURCE. *Nonlinear Dynamics*, 55:139–149, 2008.
- [58] V. Piccirillo, J. M. Balthazar, B. R. P. Jr, and J. L. P. Felix. ON A NONLINEAR AND CHAOTIC NON-IDEAL VIBRATING SYSTEM WITH SHAPE MEMORY ALLOY (SMA). *Theoretical And Applied Mechanics*, 46:597–620, 2008.
- [59] S. Prajna and A. Papachristodoulou. NONLINEAR CONTROL SYNTHESIS BY SUM OF SQUARES OPTIMIZATION: A LYAPUNOV-BASED APPROACH. pages 1–9, Melbourne, Australia, 2004.
- [60] J. Primbs, V. Nevistic, and J. Doyle. NONLINEAR OPTIMAL CONTROL: A CONTROL LYAPUNOV FUNCTION AND RECEDING HORIZON PERSPECTIVE. *Asian Journal of Control*, 1:14–24, 1999.
- [61] P. Qiang and C. Chongdu. THE INVESTIGATION OF A SHAPE MEMORY ALLOY MICRO-DAMPER FOR MEMS APPLICATIONS. *Sensors*, pages 1887–1900, 2007.

- [62] M. A. Qidawi and D. C. Lagouds. NUMERICAL IMPLEMENTATION OF A SHAPE MEMORY ALLOY THERMOMECHANICAL CONSTITUTIVE MODEL USING RETURN MAPPING ALGORITHMS. *International Journal for Numerical Methods in Engineering*, 47(6):1123–1168, 2000.
- [63] M. Rahman. PATENTS ON SUPERELASTIC SHAPE MEMORY ALLOY. *Recent Patents on Mechanical Engineering*, 1:65–67, 2008.
- [64] R. C. H. Rosario and R. C. Smith. Introduction and characterization of a functionally linked metal ion binding site at the exposed heme edge of myoglobin. *Proceedings of the National Academy of Sciences of the United States of America*, 100(7):3647–52, 2003.
- [65] T. Roubicek. MODELLING OF THERMODYNAMICS OF MARTENSITIC TRANSFORMATION IN SHAPE-MEMORY ALLOYS. *DYNAMICAL SYSTEMS*, 5402:892–902, 2007.
- [66] M. A. Savi and A. M. Braga. CHAOTIC RESPONSE OF A SHAPE MEMORY OSCILLATOR WITH INTERNAL CONSTRAINTS. In *12th Brazilian Congress of Mechanical Engineering*, pages 33–37, Rio De Janero, 1993.
- [67] M. A. Savi, A. Paiva, and P. M. Pacheco. PHENOMENOLOGICAL MODELING OF SHAPE MEMORY ALLOY THERMOMECHANICAL BEHAVIOR. Technical report, 2007.
- [68] M. A. Savi, M. A. Sa, A. Paiva, and P. M. Pacheco. TENSILE-COMPRESSIVE ASYMMETRY INFLUENCE ON SHAPE MEMORY ALLOY SYSTEM DYNAMICS. *Chaos, Solitons and Fractals*, 36:828–848, 2008.

- [69] M. Schwartz. ENCYCLOPEDIA OF SMART MATERIALS. John Wiley and Sons, 2002.
- [70] K. Tanakaa, S. Kobayashia, and Y. Satoa. THERMOMECHANICS OF TRANSFORMATION PSEUDOELASTICITY AND SHAPE MEMORY EFFECT IN ALLOYS . *International Journal of Plasticity*, 2:59–72, 1986.
- [71] H. L. Trentelman and J. C. Willems. SYNTHESIS OF DISSIPATIVE SYSTEMS USING QUADRATIC DIFFERENTIAL FORMS: PART I. *IEEE Transactions on Automatic Control*, 47:70–86, 2002.
- [72] H. L. Trentelman and J. C. Willems. SYNTHESIS OF DISSIPATIVE SYSTEMS USING QUADRATIC DIFFERENTIAL FORMS: PART II. *IEEE Transactions on Automatic Control*, 47:70–86, 2002.
- [73] M. Vasina and K. Hoder. UNCONVENTIONAL ACTUATORS FOR ROBOTICS-SHAPE MEMORY ALLOY. *2003 IEEE International Conference on Industrial Technology*, 1:190–193, 2003.
- [74] L. Wang and R. V. N. Melnik. CONTROL OF COUPLED HYSTERETIC DYNAMICS OF FERROELECTRIC MATERIALS WITH A LANDAU-TYPE DIFFERENTIAL MODEL AND FEEDBACK LINEARIZATION. *Applied Numerical Mathematics*, 18(7):074011, 2007.
- [75] L. Wang and R. V. N. Melnik. CONTROL OF COUPLED HYSTERETIC DYNAMICS OF FERROELECTRIC MATERIALS WITH A LANDAU-TYPE DIFFERENTIAL MODEL AND FEEDBACK LINEARIZATION. *Smart Materials and Structures*, 18(2009):401107, 2009.

- [76] L. X. Wang and R. V. N. Melnik. DEVELOPMENT OF A SHAPE MEMORY ALLOY ACTUATED BIOMIMETIC VEHICLE. *Smart Matrial Structures*, 9:673–683, 2000.
- [77] L. X. Wang and R. V. N. Melnik. FINITE VOLUME ANALYSIS OF NONLINEAR THERMO-MECHANICAL DYNAMICS OF SHAPE MEMORY ALLOYS. *Heat and Mass Transfer*, 43(6):535–546, 2006.
- [78] L. X. Wang and R. V. N. Melnik. MODEL REDUCTION APPLIED TO SQUARE TO RECTANGULAR MARTENSITIC TRANSFORMATIONS USING PROPER ORTHOGONAL DECOMPOSITION. *Applied Numerical Mathematics*, 57(6):510–520, 2007.
- [79] L. X. Wang and R. V. N. Melnik. MODIFYING MACROSCALE VARIANT COMBINATIONS IN A TWO-DIMENSIONAL STRUCTURE USING MECHANICAL LOADINGS DURING THERMALLY INDUCED TRANSFORMATION. *Materials Science and Engineering*, 481–482:190–193, 2008.
- [80] G. Webb, A. Kurdila, and D. Lagoudas. HYSTERESIS MODELING OF SMA ACTUATORS FOR CONTROL APPLICATIONS. *Journal of Intelligent Material Systems*, 9:432–448, 1998.
- [81] Z. G. WEI and R. SANDSTROM. REVIEW: SHAPE-MEMORY MATERIALS AND HYBRID COMPOSITES FOR SMART SYSTEMS. *Journal of Materials Science*, 33:3743–3762, 1998.
- [82] J. C. Willems. DISSIPATIVE DYNAMICAL SYSTEMS. *European Journal of Gontrol*, 13:134–151, 2007.
- [83] L. Yan and B. Liu. STABILIZATION WITH OPTIMAL PERFORMANCE FOR DISSI-

PATIVE DISCRETE-TIME IMPULSIVE HYBRID SYSTEMS. *Advances in Difference Equations*, 2010:1–15, 2010.

[84] T. Yoshida. SUPERELASTIC DENTAL AU-CU-ZN ALLOYS. <http://www.docstoc.com/docs/47466953/Superelastic-Dental-Au-Cu-Zn-Alloys—Patent-4690799>, 1987.

[85] Y. Zhao, M. Taya, Y. Kang, and a. Kawasaki. COMPRESSION BEHAVIOR OF POROUS NiTi SHAPE MEMORY ALLOY. *Acta Materialia*, 53(2):337–343, 2005.

[86] Y. Zheng and B. M. Buang. SUPERELASTIC AND THERMALLY ACTIVATED TiNi ALLOYS AND THEIR APPLICATIONS. *Material Science Forum*, 394–395:57–60, 2002.